STUDY OF CAPABILITIES OF GROUND BASED SENSORS FOR DETECTION OF SMALL TECHNOGENIC PARTICLES AND ASTEROIDS

Final Report

by

the Centre for Program Studies

Russian Academy of Sciences

SPC-93-4077

Moscow

May, 1994

The Report discusses the problem of detection of small-size space debris and asteroids.

Analysis of existing Russian ground based and space based sensors is provided us to perform the assigned objectives are selected:

- a cm-band BMD radar;
- dm-band BMD radar's;
- an experimental mm/cm-band radar complex;
- a mobile multipurpose telescope;
- visible\UV-band on-board space sensors (one is on-orbit now and the second is being prepared for launch to MIR station);
- optical telescopes of the observatories network of the Russian Academy of Sciences.

Results experimental detection and identification of small-size space objects obtained by four BMD radar's are presented.

A technique for the experiment on possible detection of asteroids is proposed. It involves use of optical sensors and high-potential radar's.

The Report was prepared by the Centre for Program Studies, Russian Academy of Sciences according to the special contract SPC-93-4077. This work was done under the leadership of Prof. G.M.Chernyavskiy, Director of the Centre, with a task group of Russian experts participating in the study.

DISCLAIMER NOTICE

THIS DOCUMENT IS BEST QUALITY AVAILABLE. THE COPY FURNISHED TO DTIC CONTAINED A SIGNIFICANT NUMBER OF PAGES WHICH DO NOT REPRODUCE LEGIBLY.

REPORT DOCUMENTATION PAGE

Form Approved OMB No. 0704-0188

1. AGENCY USE ONLY (Leave blank)	2. REPORT DATE	3. REPORT TYPE AND DATES COVERED
	May 1994	Final Report,

4. TITLE AND SUBTITLE

Study of Capabilities of Ground Based Sensors for Detection of Small Technogenic Particles and Asteroids

5. FUNDING NUMBERS

F6170893W0987

6. AUTHOR(S)

Prof Grigoriy M. Chernyavskiy

7. PERFORMING ORGANIZATION NAME(S) AND ADDRESS(ES)

Russian Academy of Sciences
Center for Program Studies
84/32 Profsoyuznaya Ulitsa
Moscow 117810, Russia

8. PERFORMING ORGANIZATION REPORT NUMBER

SPC-93-4077

9. SPONSORING/MONITORING AGENCY NAME(S) AND ADDRESS(ES)

EOARD
PSC 802 BOX 14
FPO AE 09499-0200

10. SPONSORING/MONITORING AGENCY REPORT NUMBER

SPC-93-4077

11. SUPPLEMENTARY NOTES

12a. DISTRIBUTION/AVAILABILITY STATEMENT

Unlimited

12b. DISTRIBUTION CODE

13. ABSTRACT (Maximum 200 words)

The report discusses the problem of detection of small-size space debris and asteroids. Analysis of existing Russian ground based and space based sensors is provided us to perform the assigned objectives are selected: a cm-band BMD radar, dm band BMD radar, an experimental mm/cm-band radar complex, a mobile multipurpose telescope, visible/UV-band on-board space sensors (one is on-orbit now and the second is being prepared for launch to MIR station), optical telescopes of the observatories network of the Russian Academy of Sciences. Results: experimental detection and identification of small-size space objects obtained by four BMD radars are presented. A technique for the experiment on possible detection of asteroids is proposed. It involves use of optical sensors and high-potential radars.

14. SUBJECT TERMS

15. NUMBER OF PAGES

58

16. PRICE CODE

17. SECURITY CLASSIFICATION OF REPORT	18. SECURITY CLASSIFICATION OF THIS PAGE	19, SECURITY CLASSIFICATION OF ABSTRACT	20. LIMITATION OF ABSTRACT
UNCLASSIFIED	UNCLASSIFIED	UNCLASSIFIED	UL

Table of contents

Introduction

Detection and identification of small technogenic orbital debris and asteroids constitutes a difficult problem for science and technology. Its solution depends strongly on availability of necessary sensor systems. Contemporary operational Earth orbit surveillance systems have certain limitations - both by the size of detected debris (not less than 10 cm).

Employment of the Haystack radar was a great step forward in investigations of the small-size debris (1 - 10 cm). The Haystack data provided the basis for updating the fidelity of the NASA Debris Environment Model and for its employment is spacecraft design. Information from the Haystack contains certain results that differ from those given in earlier forecasts. Therefore it becomes necessary to perform a number of complementary space surveillance experiments, including those done independently from the Haystack. Development and design of new sensor systems requires substantial investments. So quite naturally we come to an evident solution: possible employment of operational sensor systems (including Russian assets) for detection of low-contrast objects, such as small size fraction of space debris and asteroids.

Our Report gives a discussion of this problem.

Chapter 1.
Capabilities of Ground based High Potential Radar's for Detection of Small Technogenic Particles

1.1. Capabilities of the Russian space surveillance assets

Existing Russian space surveillance assets include (Fig. 1.1.1):

• High-potential meter-band radar's, which work as an integral part of the missile attack warning system and are deployed near Pechora (Northern Russia), Olenegorsk (Kola Peninsula), Skrunda (Latvia), Mukatchevo (West Ukraine), Sevastopol (Crimea), Kutkashen (Azerbaijan), Balkhash (Kazakhstan), Irkutsk (East Siberia).

• Optical (opto-electronic) telescopes integrated in the RAS network of observatories: Zvenigorod (Moscow Region), Simeiz (Crimea), Zelenchukskaya (North Caucasus), Irkutsk (Siberia), Ekaterinburg (Ural), Dushanbe (Tadjikistan).

To obtain data on space objects (SO) there are also employed (regularly or episodically):

• High-potential radar's operating in the long-wave segment of the dm-band, and operated by the BMD system (Chekhov, Moscow Region);

• An Experimental cm-band radar (Ust-Kamchatsk, Kamchatka Peninsula);

• Radiotechnic systems for processing of the co-ordinate information received from active space objects.

These systems enable compiling and updating of the Space Objects Catalogue containing over 5,000 objects larger than 10 cm in size (at low orbits) and larger than 1 m (at geostationary orbits). Detection of more small objects in space represents a serious scientific and technological problem.

The radar cross section (RCS) of such objects essentially depends on the radar wavelength and does not exceed 18 dB/m^2 in the RF band range of 3 to 23 cm.

Figs. 1.1.2 - 1.1.8 illustrates the estimated dependence between the RCS for a quasi spherical-shape fragment and its size given for one of typical frequency bands of radar's. Most preferable RF band ranges for detection of small-size space fragments include mm-band, cm-band and the short-wave segment of the dm-band. The figures indicates, that for detection of debris at distances of 600 to

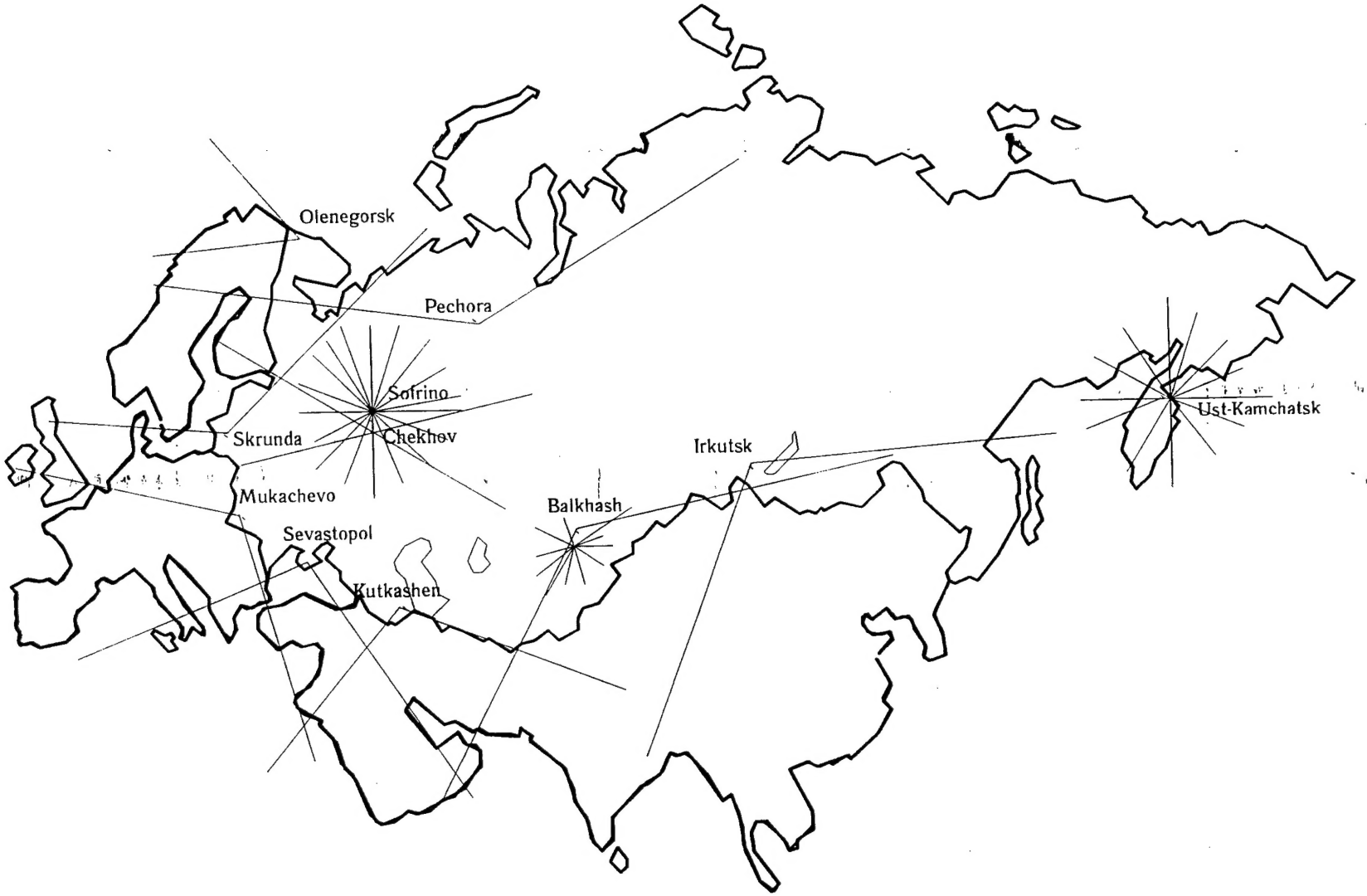

Fig. 1.1.1. Space Curveillance Assets of Russia.

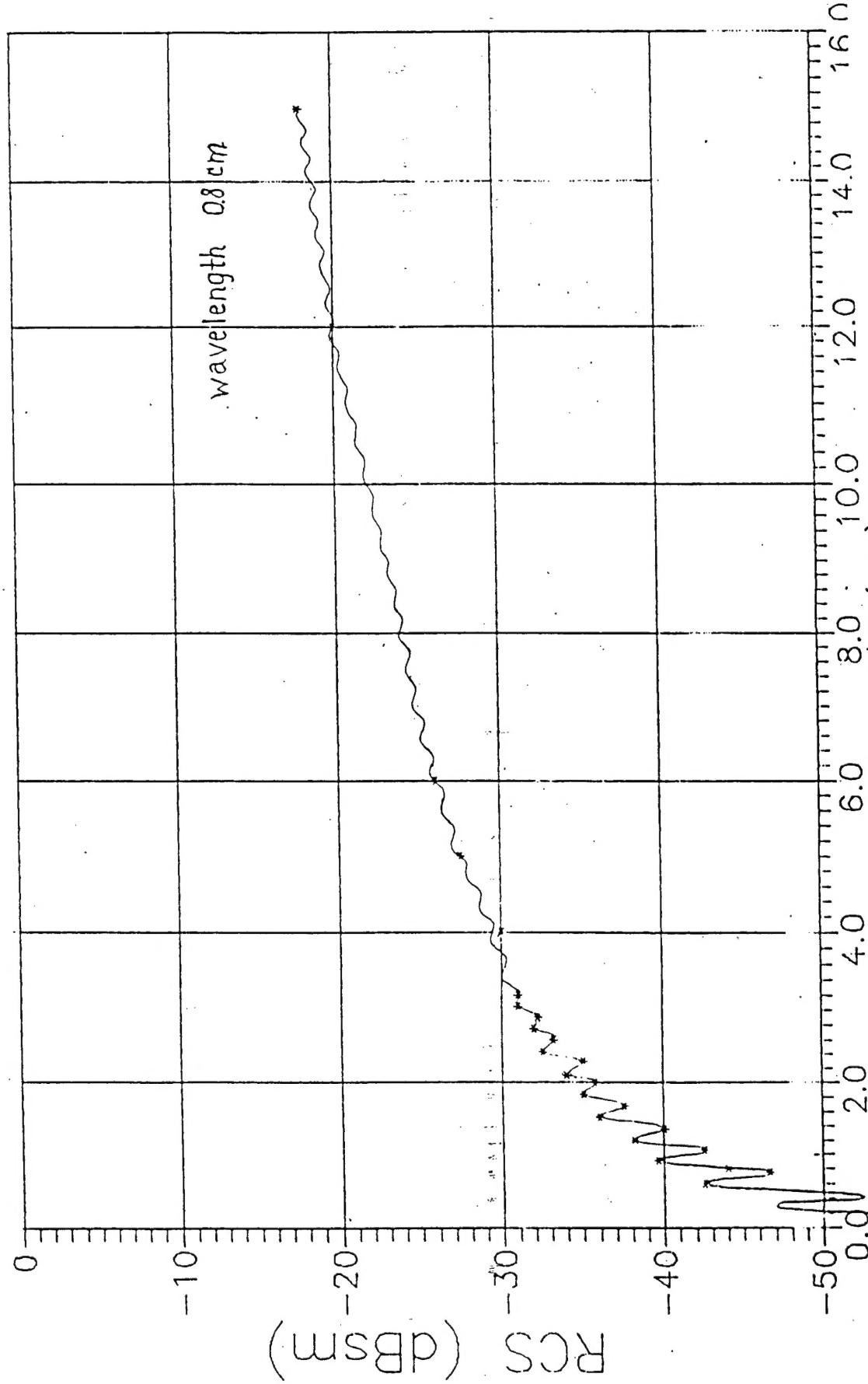

Fig. 1.1.2 Calculated RCS/DIA of Objects.

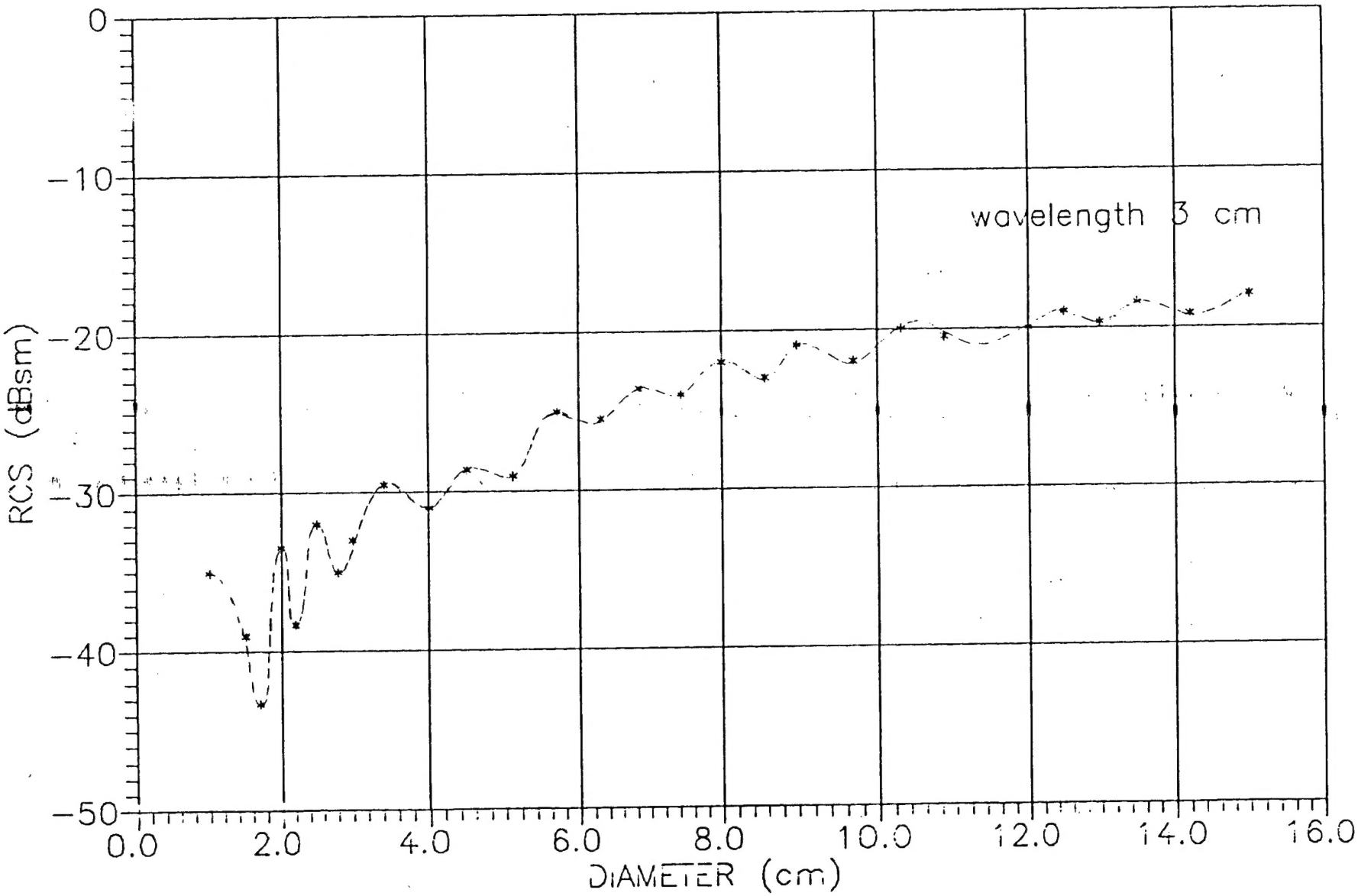

Fig. 1.1.3 Calculated RCS/DIA of Objects.

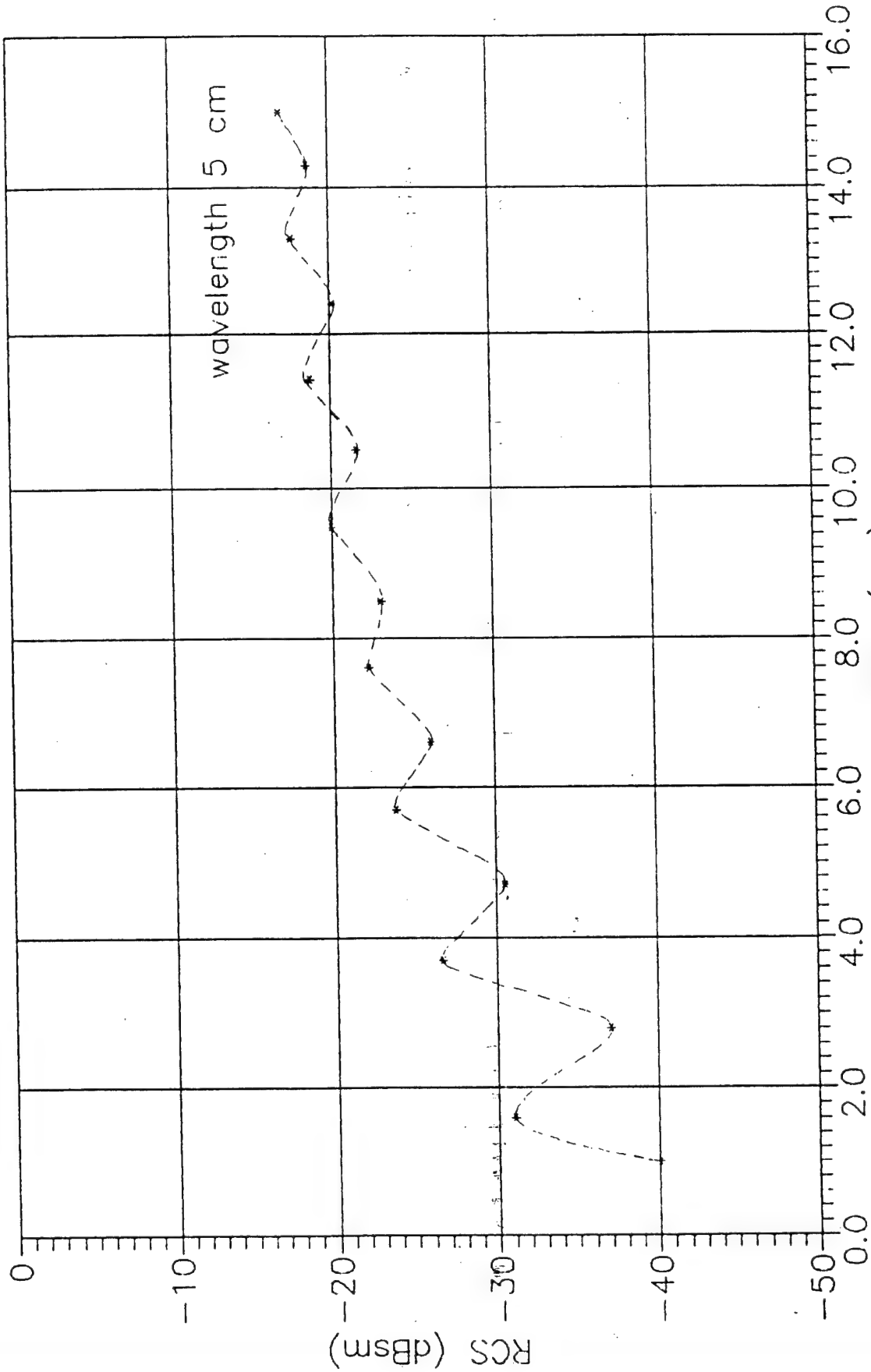

Fig. 1.1.4 Calculated RCS/DIA of Objects.

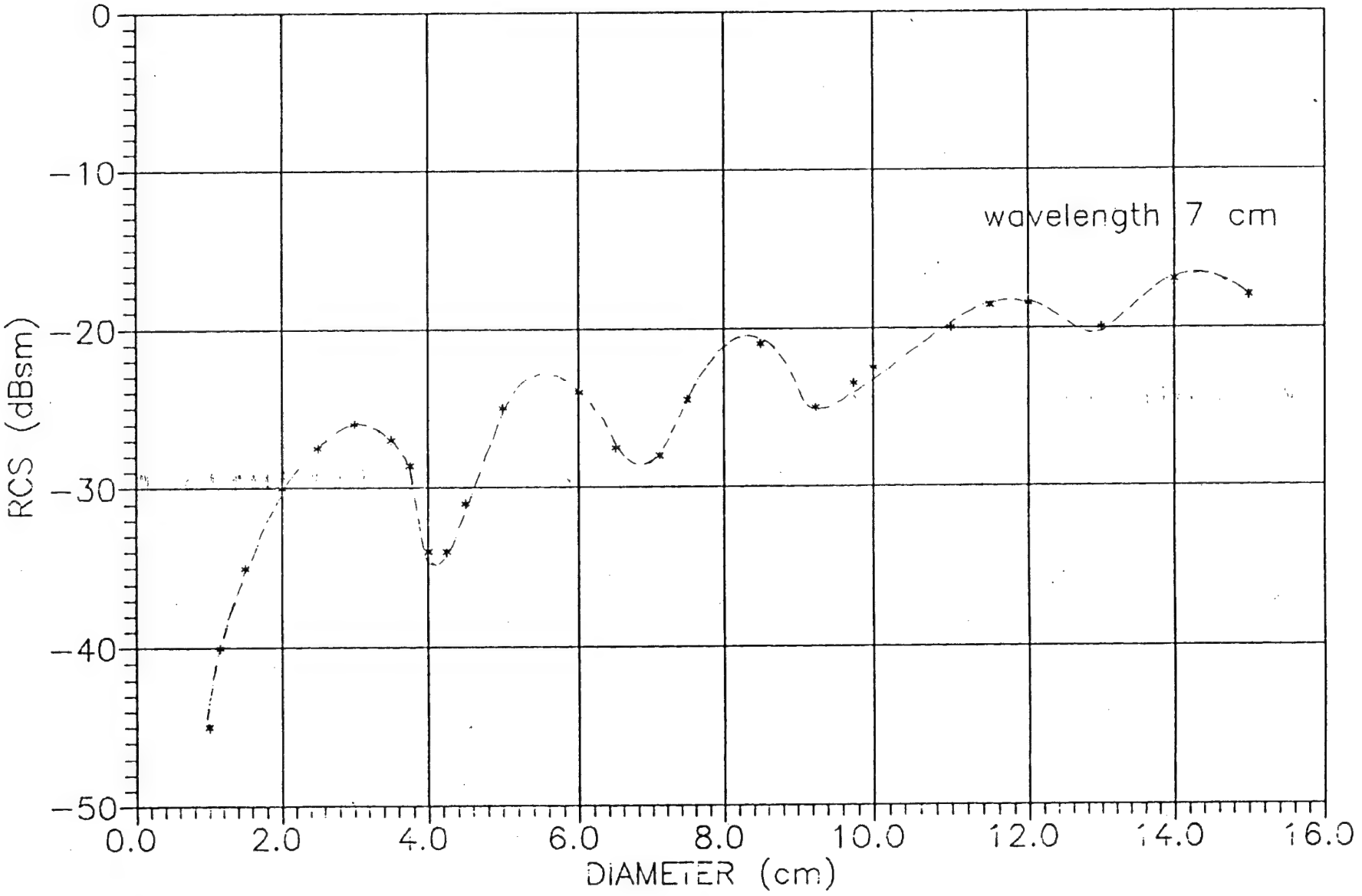

Fig. 1.1.5 Calculated RCS/DIA of Objects.

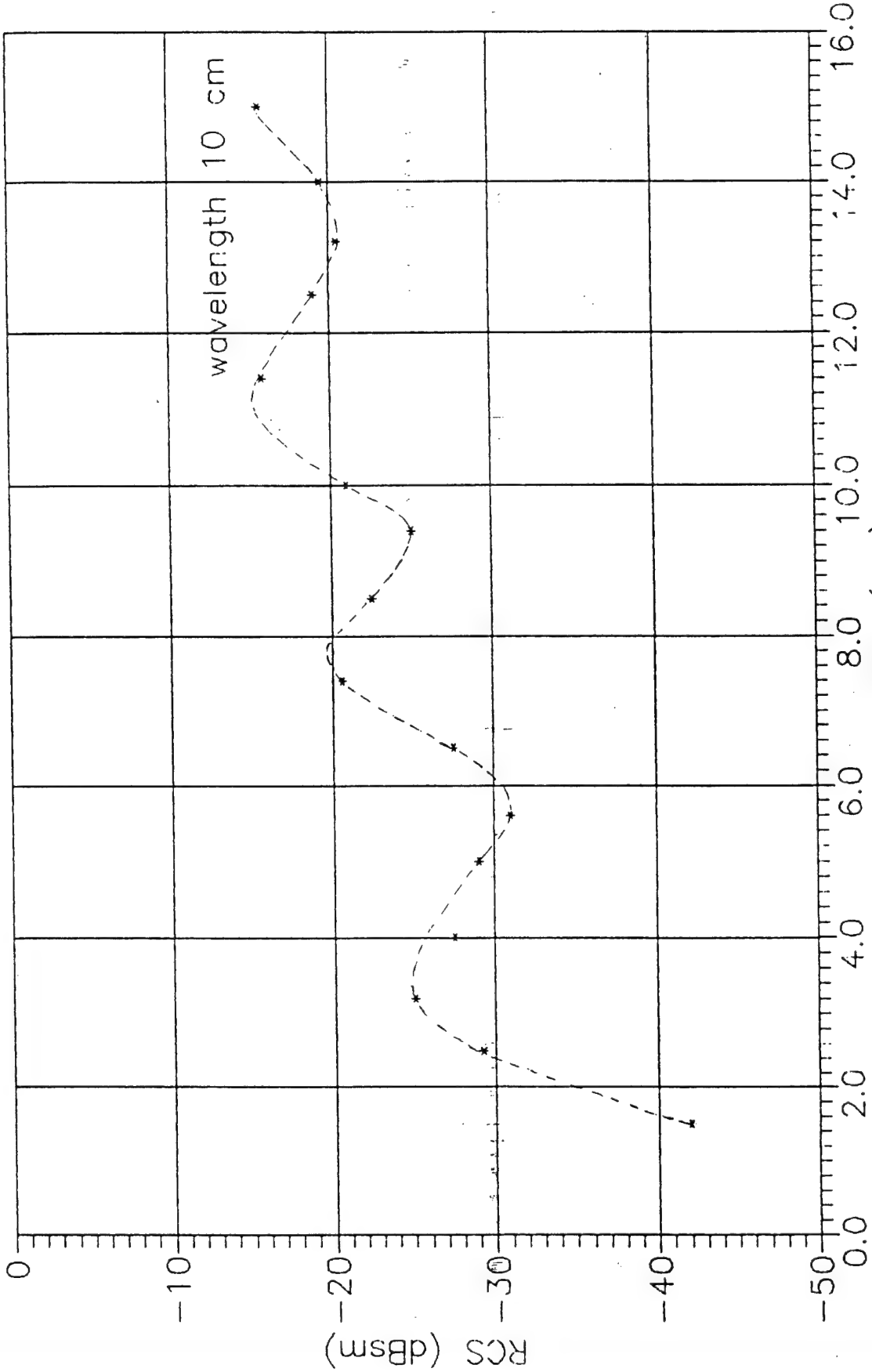

Fig. 1.1.6 Calculated RCS/DIA of Objects.

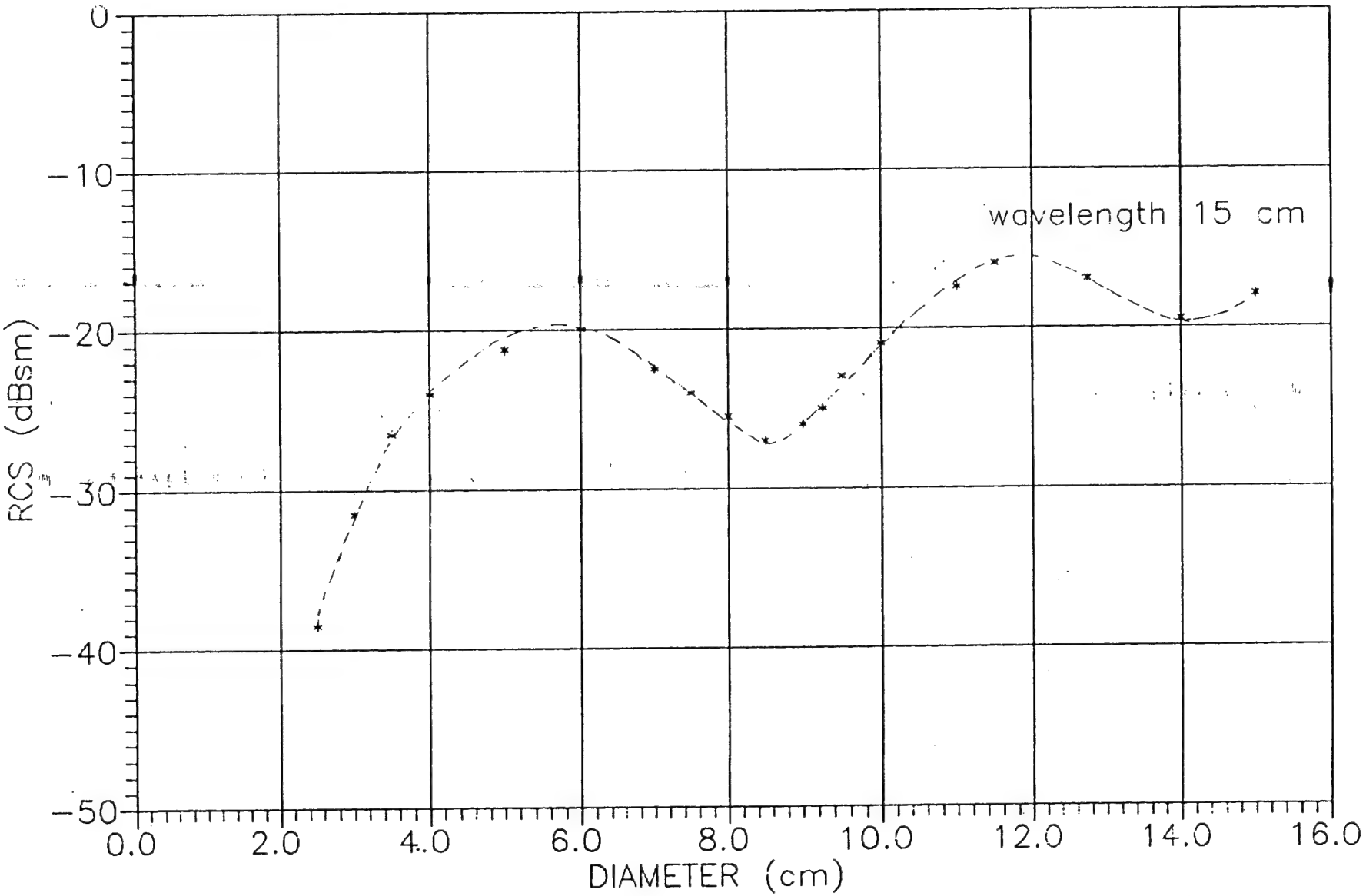

Fig. 1.1.7 Calculated RCS / DIA of Objects.

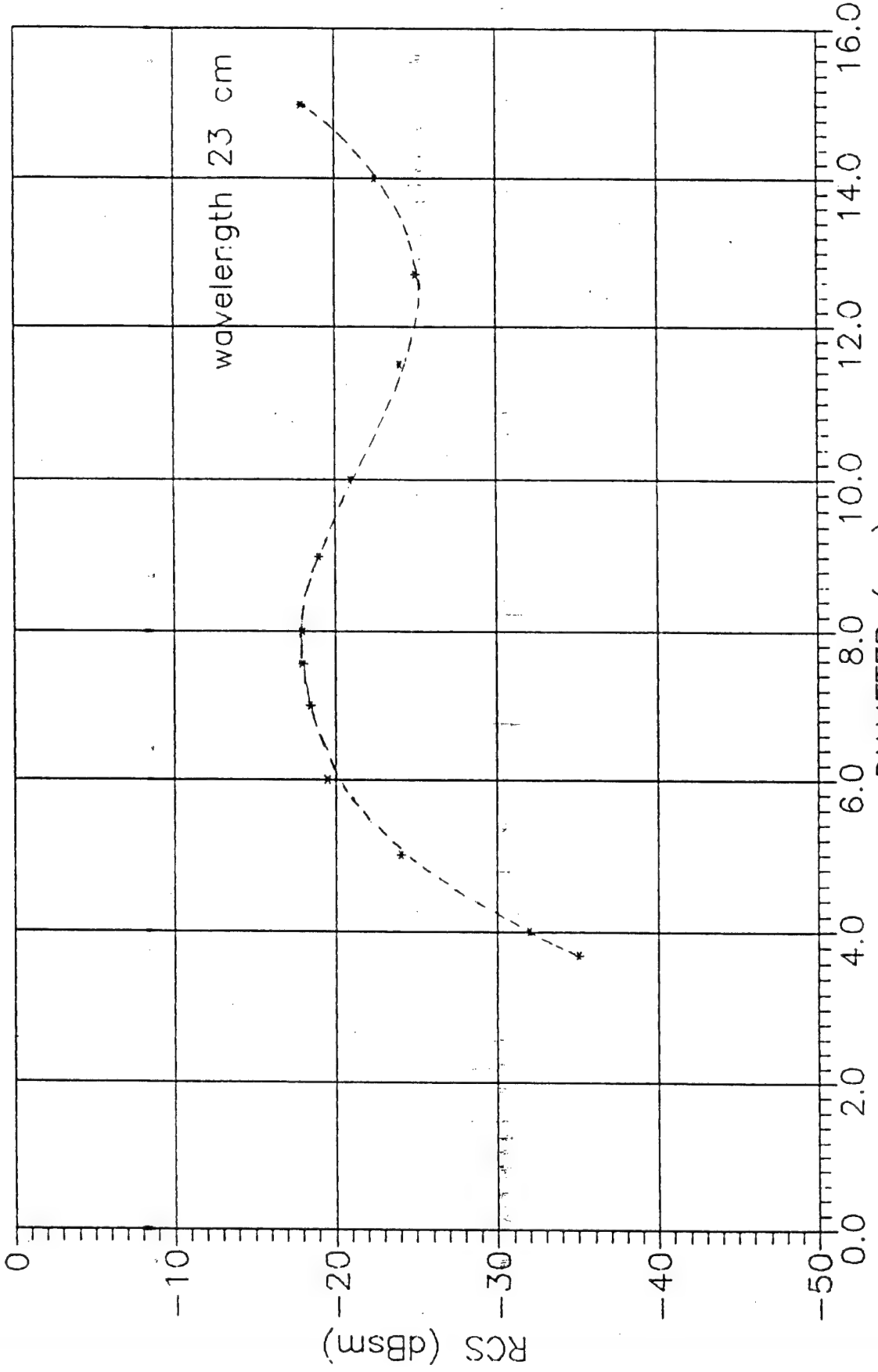

Fig. 1.1.8 Calculated RCS/DIA of Objects.

1200 km, potential of the radar must be not less than 35 dB. Some Russian high-potential radar's of dm-, cm- and mm-bands satisfy these requirements quite adequately.

1.2. Capabilities of the cm-band radar

The BMD system radar operating in the long-wave segment of the cm-band is located at Sofrino, Moscow Region.

This is a pulse radar with a fixed phase array antenna, capable of surveying the upper near-Earth space (NES) hemisphere. Estimated capabilities of the radar operating in the space debris (SD) detection/surveying mode are shown in Fig. 1.2.1.

Some algorithmic improvements have been made for experimental evaluation of these radar capabilities. Namely, a special mode of LEO surveillance with the incoherent accumulation of up to 10 echo-signals was added into the operational software of the system. The purpose of these improvements was to detect small-size (< 10 cm) SOs and to track them up to their exit from the radar observation zone. After completion of these improvements , the test experiment was performed.

115 observation sessions with duration from 15 to 80 minutes were carried out. The total duration of the experiment was 85 hours. During this experiment the spheres with calibrated dimensions (5 cm, 10 cm and 15 cm in diameter) were flown in the LEO (in the framework of ODERACS program). It gave us a possibility to employ two modes of observations: first- to observe an arbitrary volume of space, and second - to observe volumes of space with calibrated spheres in them. This approach assured a reliable estimation of the results obtained. Fig. 1.2.1 shows the typical data obtained by the experiment. A deviation from the calculated curve is explained by specific parameters of the observed zone: position of 500 - 600 km and depth of ≈ 100 km chosen for the experiment involving observation sessions with the calibrated spheres. The detected SOs have been tracked reliably up to the moment of exit from the radar observation zone (> 1500 km).

Characteristics of reflected signals (the amplitude and two quadrature components) have been measured in the course of the experiment, and the RCS of targets (RCS-T) was evaluated. The errors of RCS-T measurements did not exceed 1 dB.

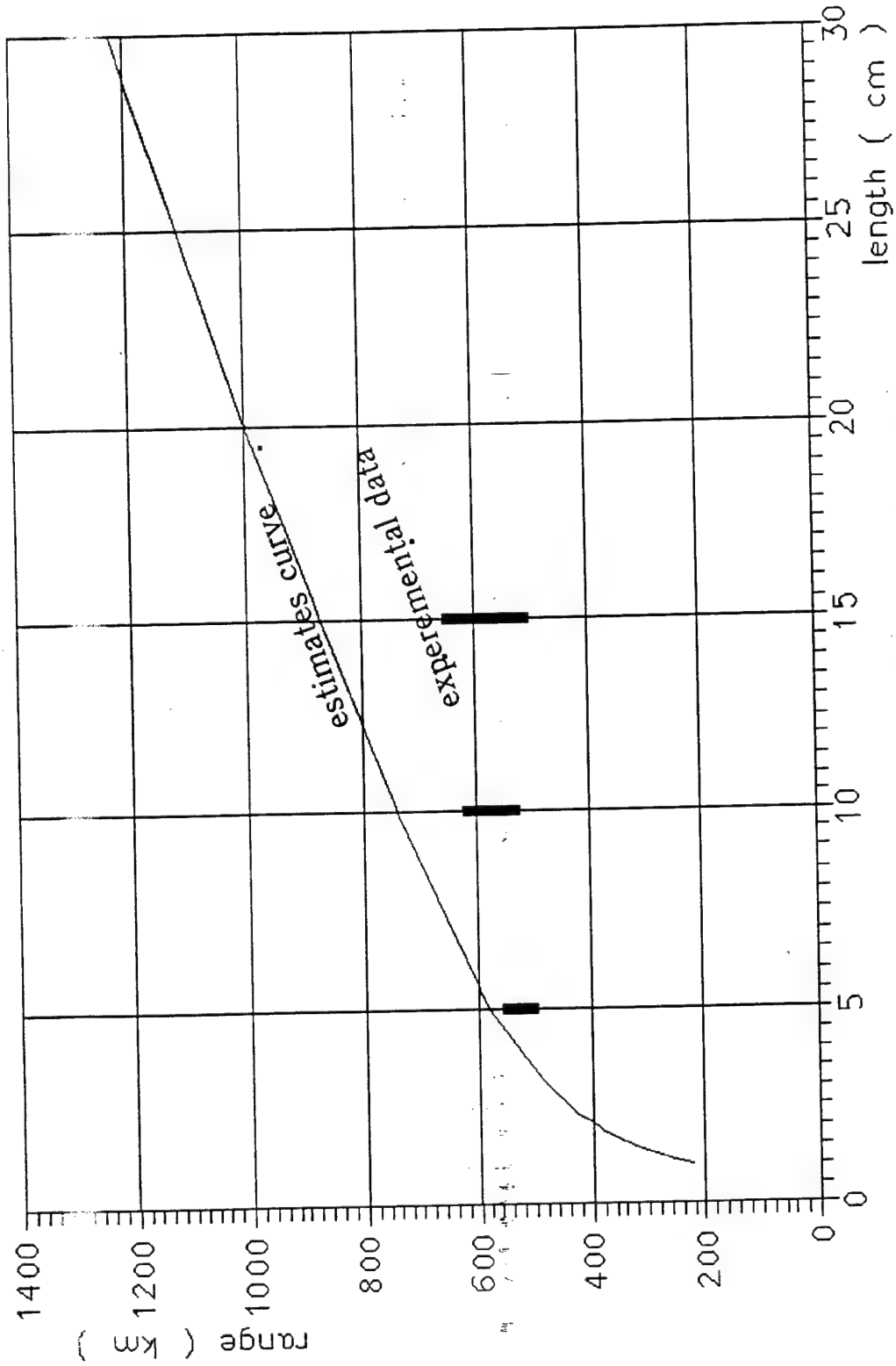

Fig. 1.2.1. Detection capabilities of the cm-band radar
- estimates and experimental data.

Figs. 1.2.2 - 1.2.5 shows several segments of the observed tracks of the radar calibrating spheres trajectories.

Figs. 1.2.6 - 1.2.16 presents the values of the RCS-T estimations normalised with respect to their calculated parameters.

Fig. 1.2.17 present the sets of RCST estimations for three objects normalised with respect to the 10 cm sphere.

Most complete utilisation of the radar's potential for detection of small-size objects and asteroids is possible under the following conditions:

- introduction of the noncogerent accumulation of maximum possible number signals (in our case it is 100 signals);
- Employment of the narrow-angle mode of illumination (less than 1 square degree) using external target designation.

The estimated ranges for detection of a metal SO for this mode of operations are shown in Fig. 1.2.18.

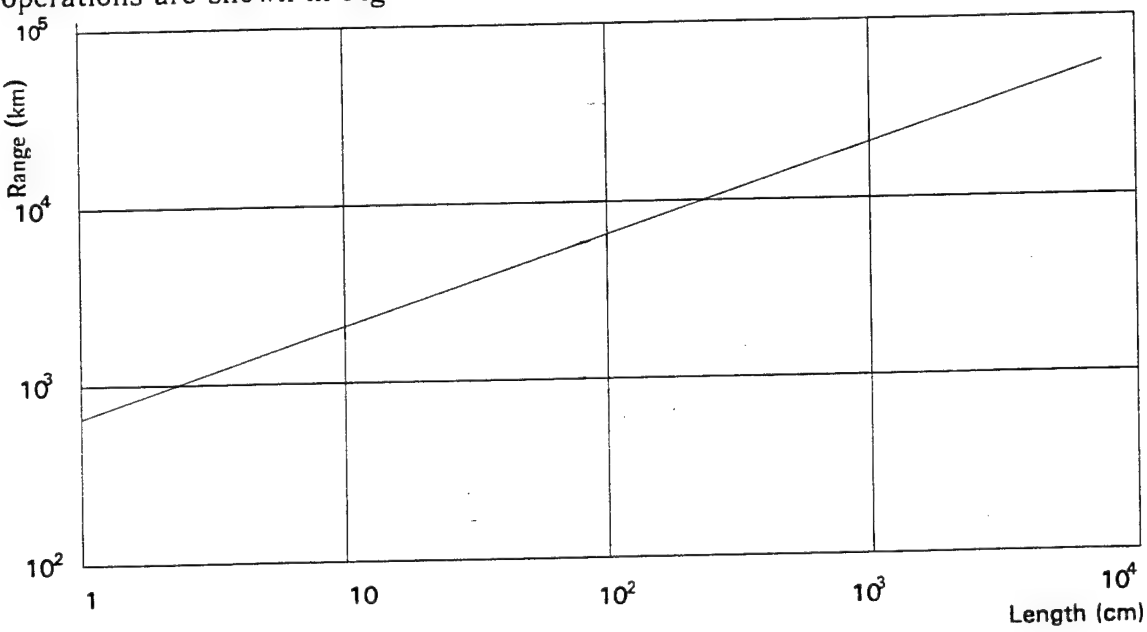

Fig. 1.2.18. Estimated detection capabilities of the cm-band radar.

For asteroids with a reflection index lower than that of a metal object, the detection borders shown in Fig. 1.2.17 are achieved for bodies of larger size. So, at the 20,000 km border the size of a body detected by radar should be not less than the following:

20...30 m - for stone asteroids (reflection index is 0.15...0.3);

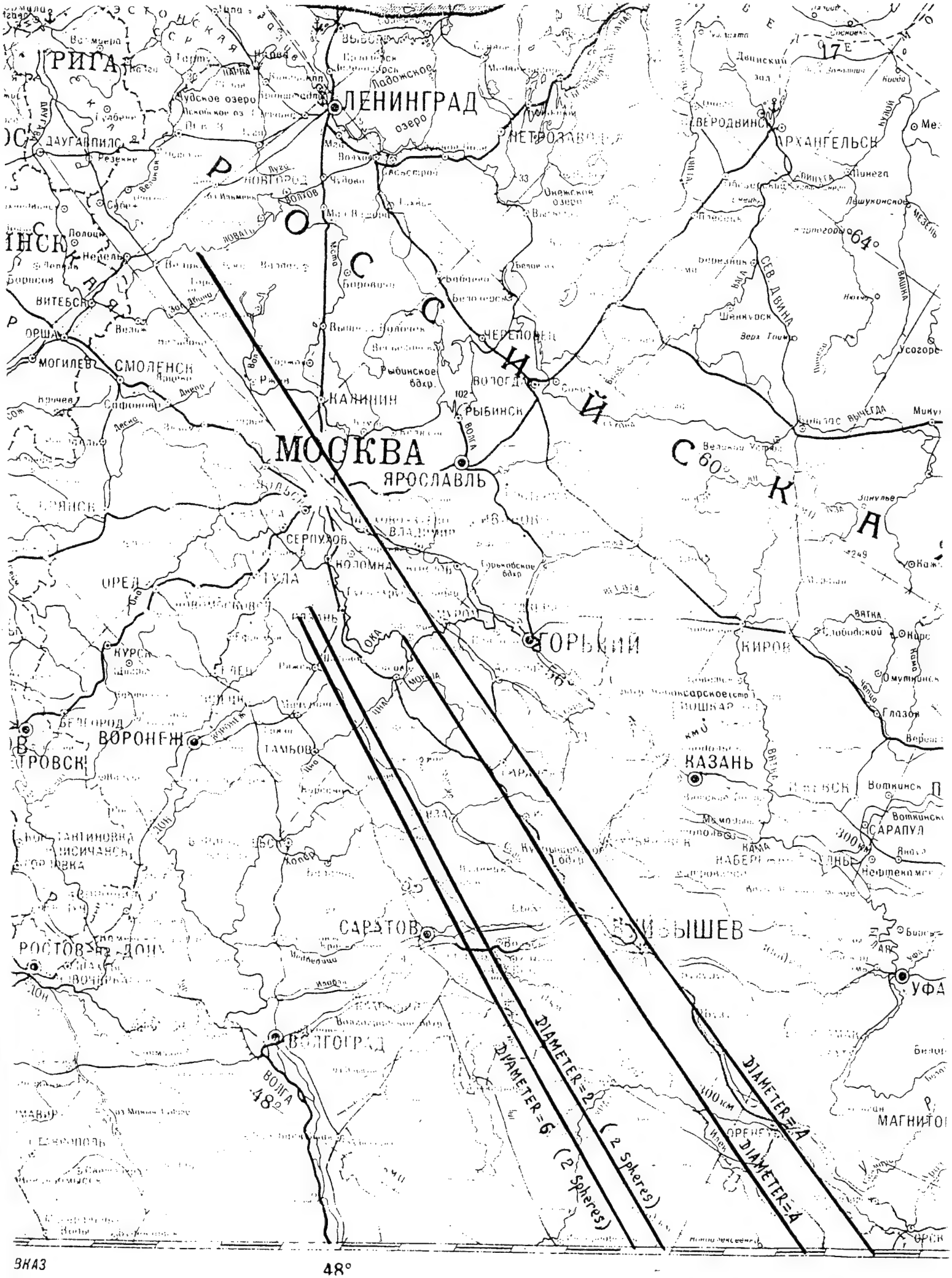
РИГА
ЛЕНИНГРАД
Ладожское озеро
Чудское озеро
ДАУГАВПИЛС
НОВГОРОД
ВОЛХОВ
ВИТЕБСК
ОРША
МОГИЛЕВ
СМОЛЕНСК
КАЛИНИН
Рыбинское вдхр.
РЫБИНСК
ВОЛОГДА
ЧЕРЕПОВЕЦ
Онежское озеро
МОСКВА
ЯРОСЛАВЛЬ
СЕРПУХОВ
КОЛОМНА
ТУЛА
ОРЕЛ
КУРСК
ВОРОНЕЖ
ТАМБОВ
САРАТОВ
РОСТОВ-НА-ДОНУ
ВОЛГОГРАД
ГОРЬКИЙ
КИРОВ
КАЗАНЬ
САРАПУЛ
КУЙБЫШЕВ
УФА
МАГНИТОГ
АРХАНГЕЛЬСК
СЕВЕРОДВИНСК
ВЫЧЕГДА
ВЯТКА
ОКА
ВОЛГА
КАМА
СЕВ. ДВИНА
РОССИЙСКАЯ СОВЕТСКАЯ
ДИАМЕТР=6 (2 Spheres)
DIAMETER=6 (2 Spheres)
DIAMETER=2 (2 Spheres)
DIAMETER=4
300км
64°
60°
48°
17 E

ВНАЗ

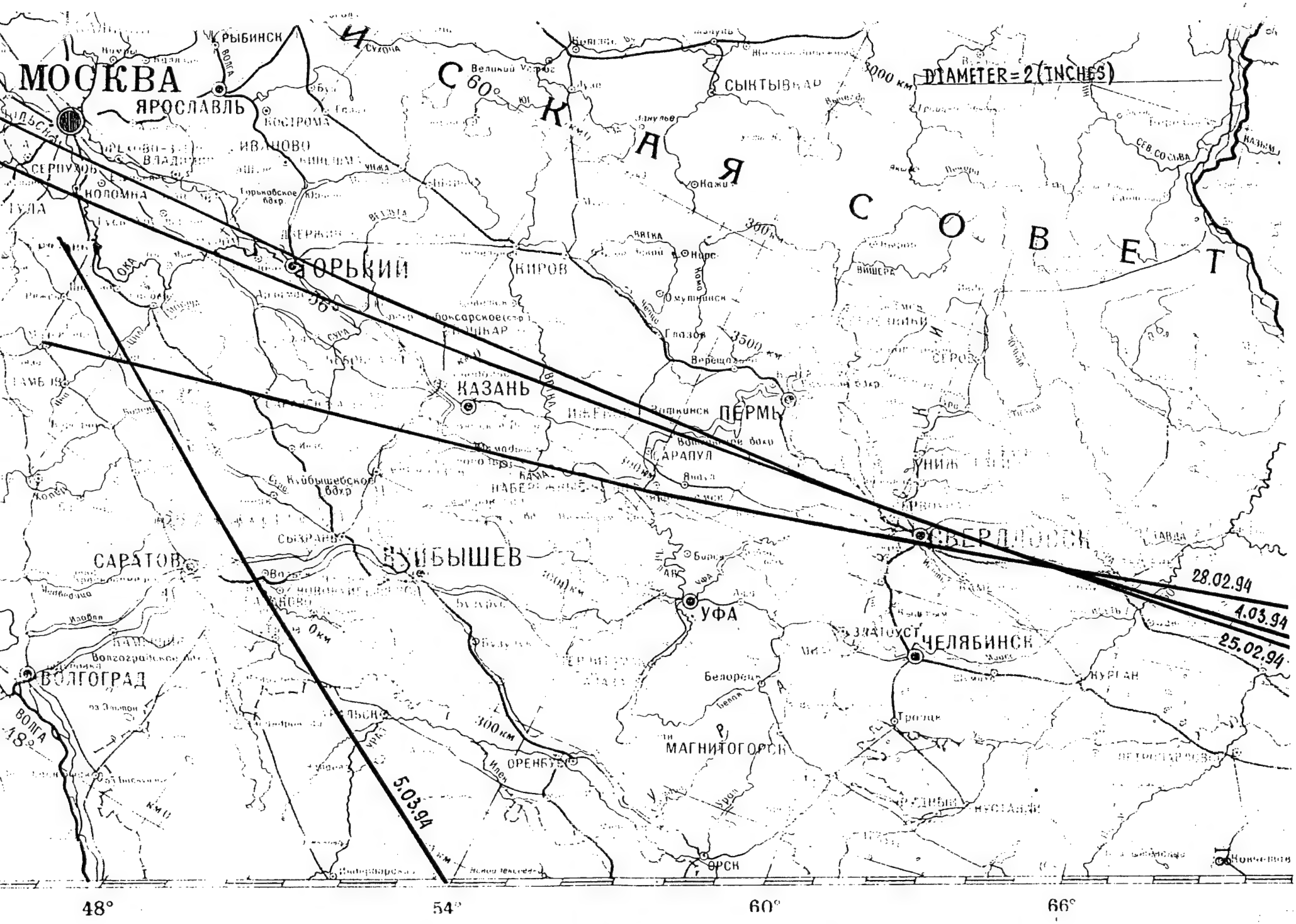

Fig. 1.2.3 Observed Tracks of Space Objects.

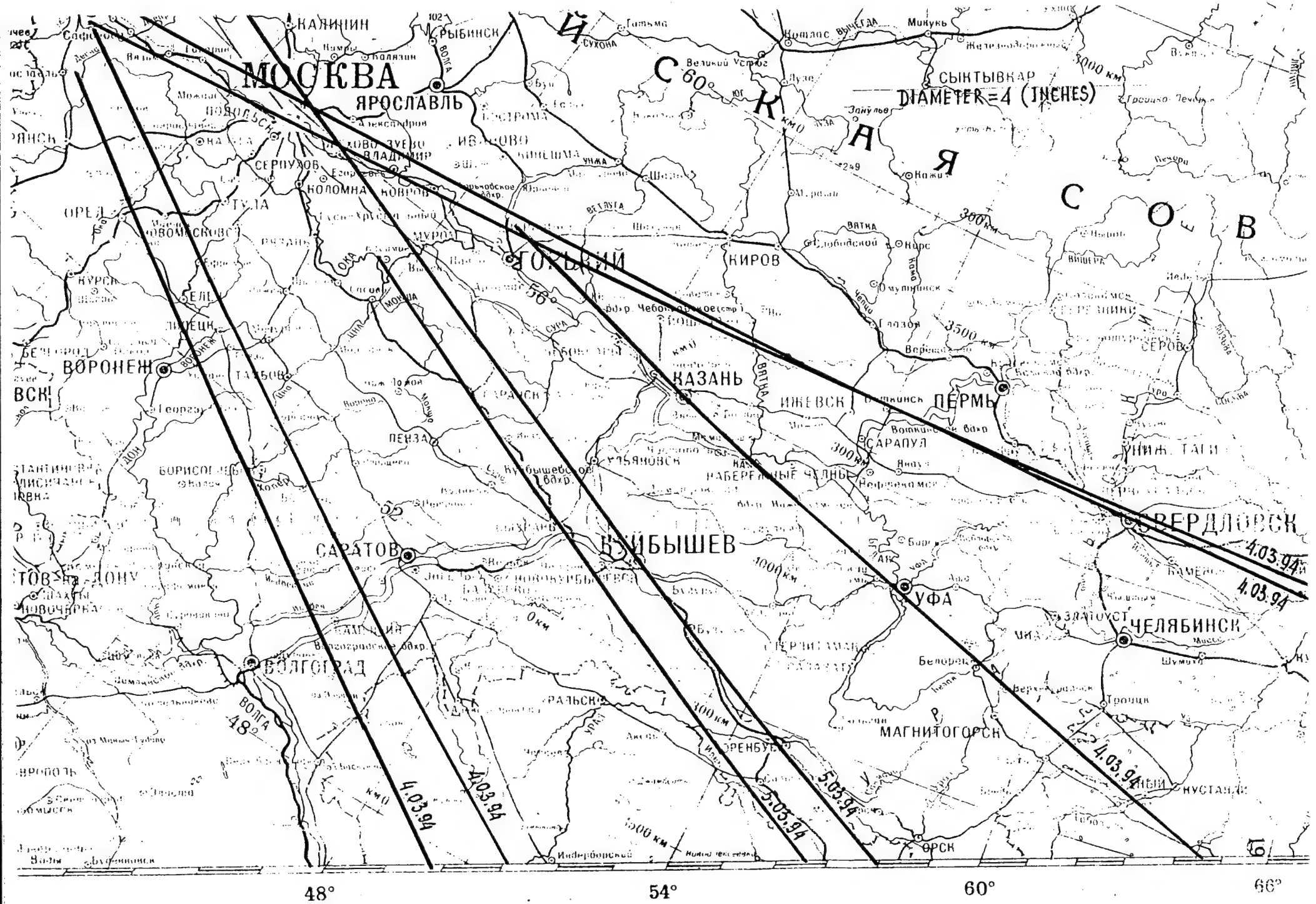

Fig. 1.2.4 Observed Tracks of Space Objects.

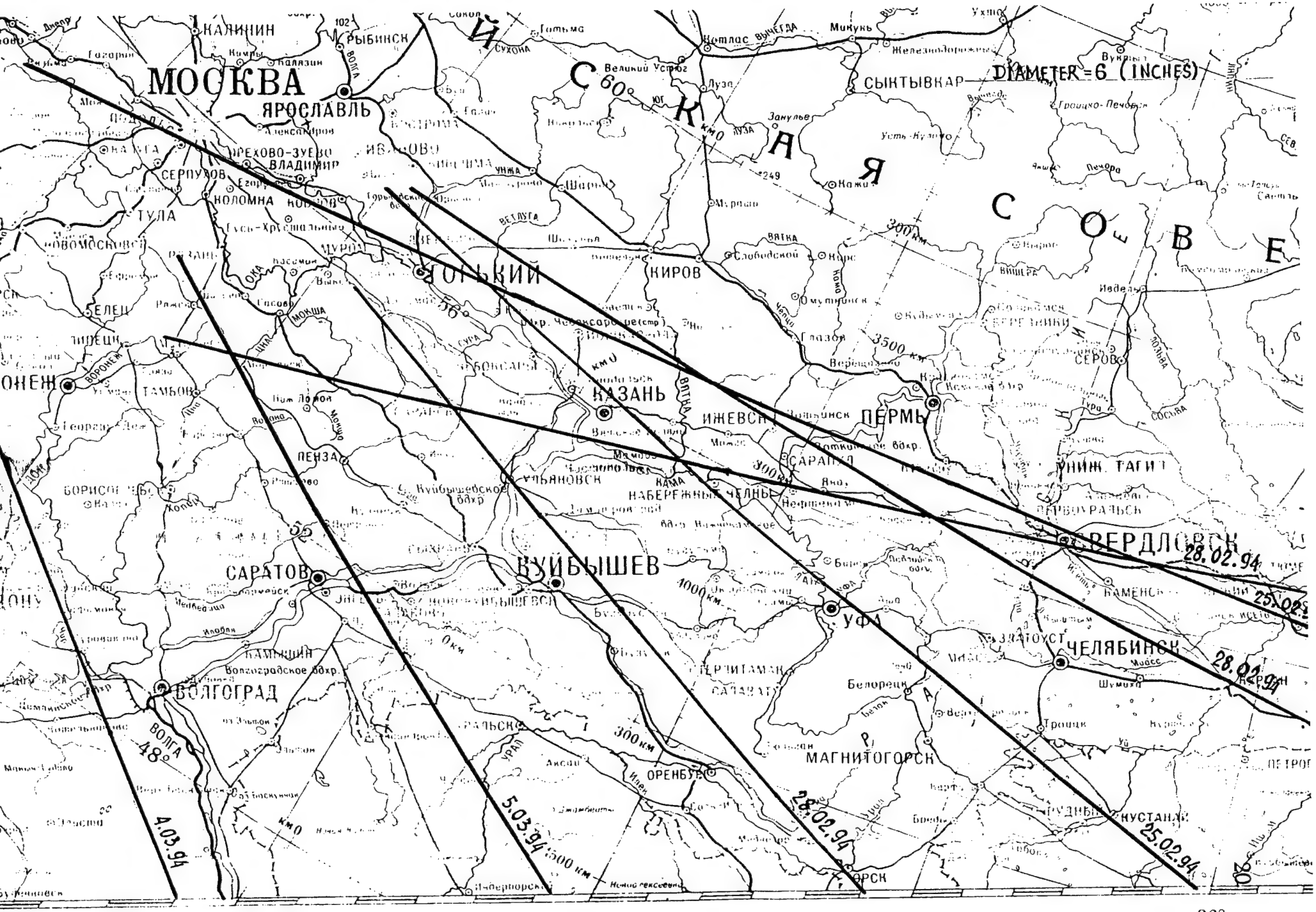

Fig 1.2.5 Observed Tracks of Space Objects.

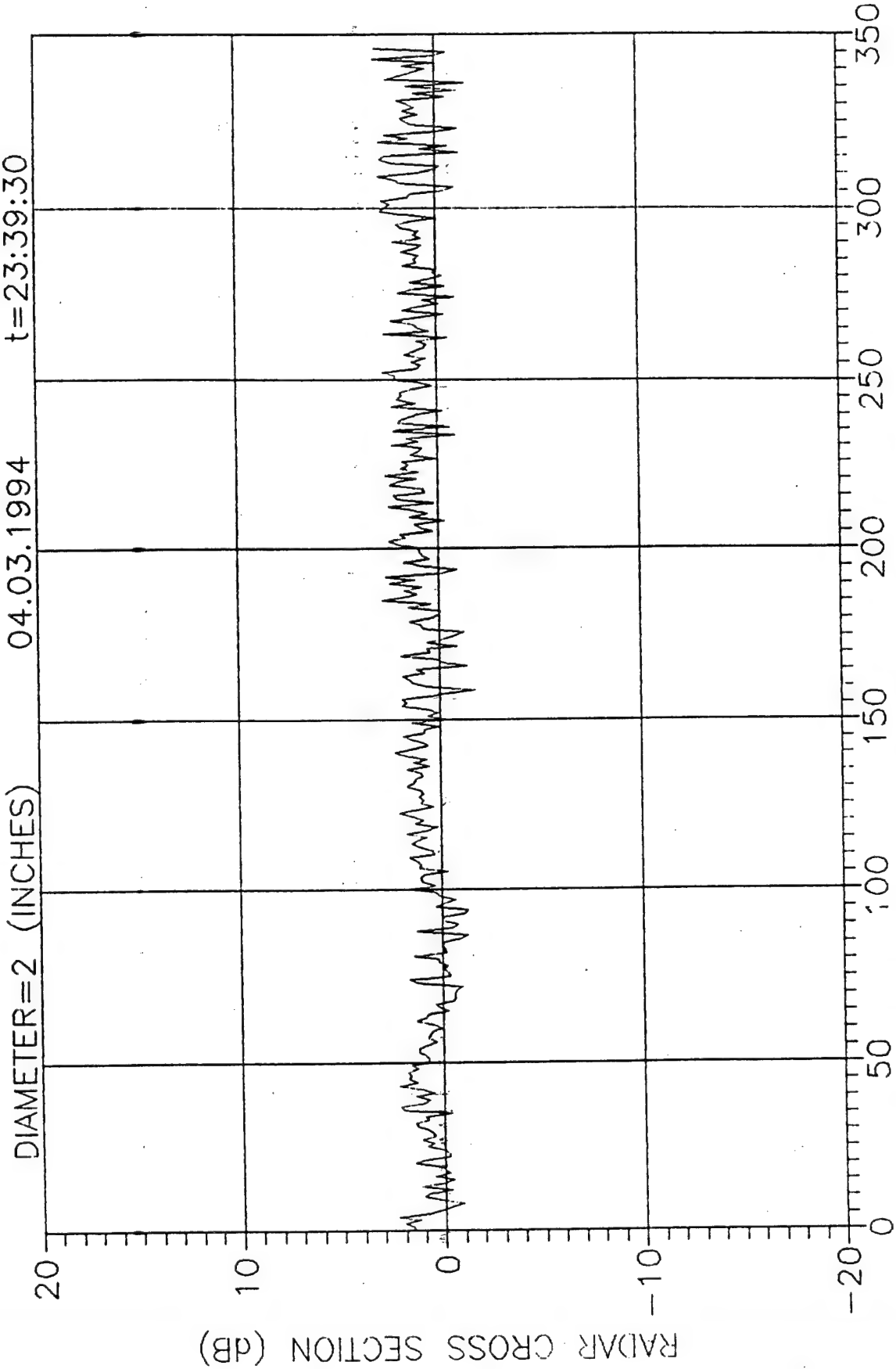

Fig. 1.2.6 Experimental RCS values

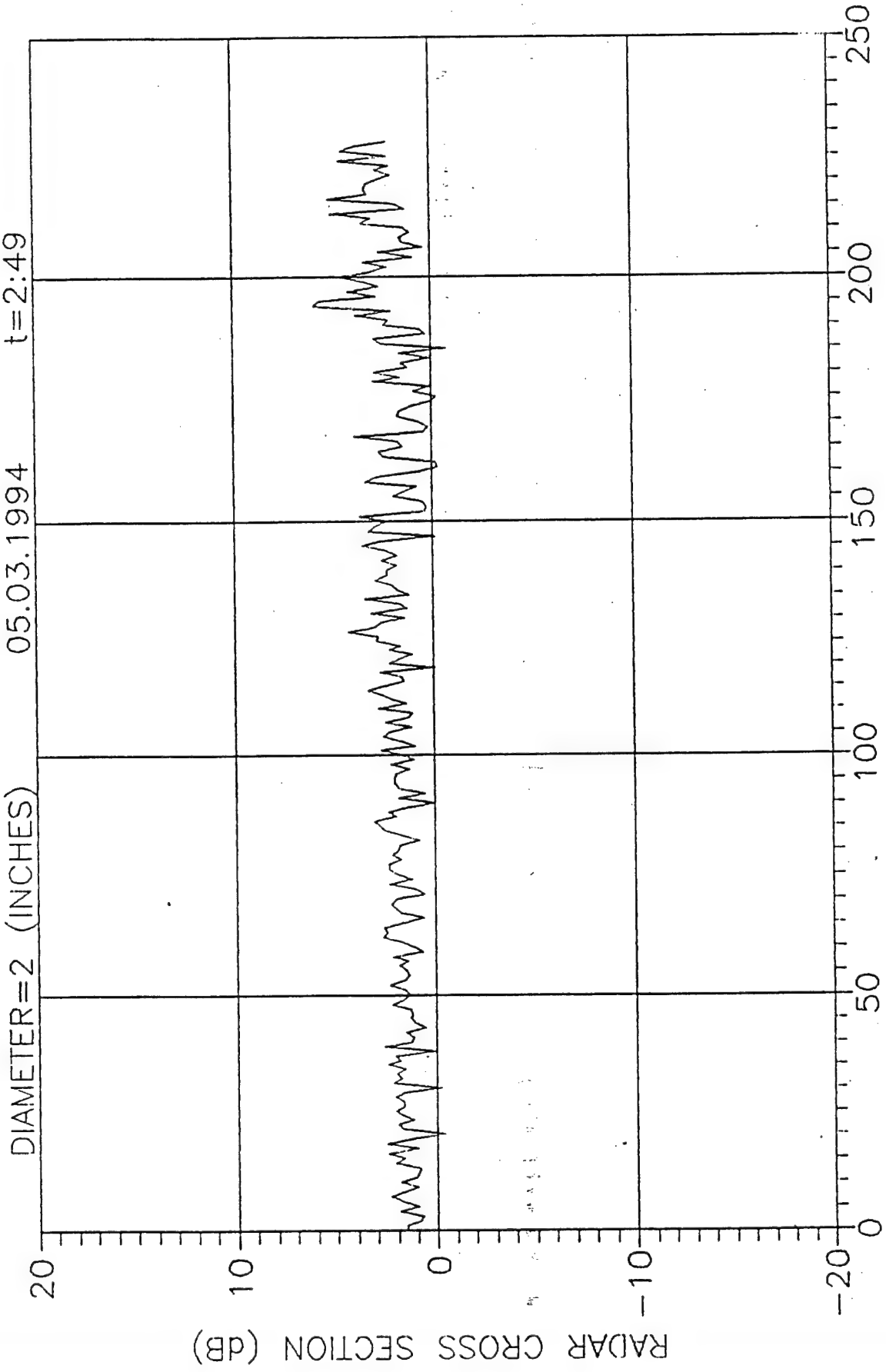

Fig. 1.2.7 Experimental RCS values

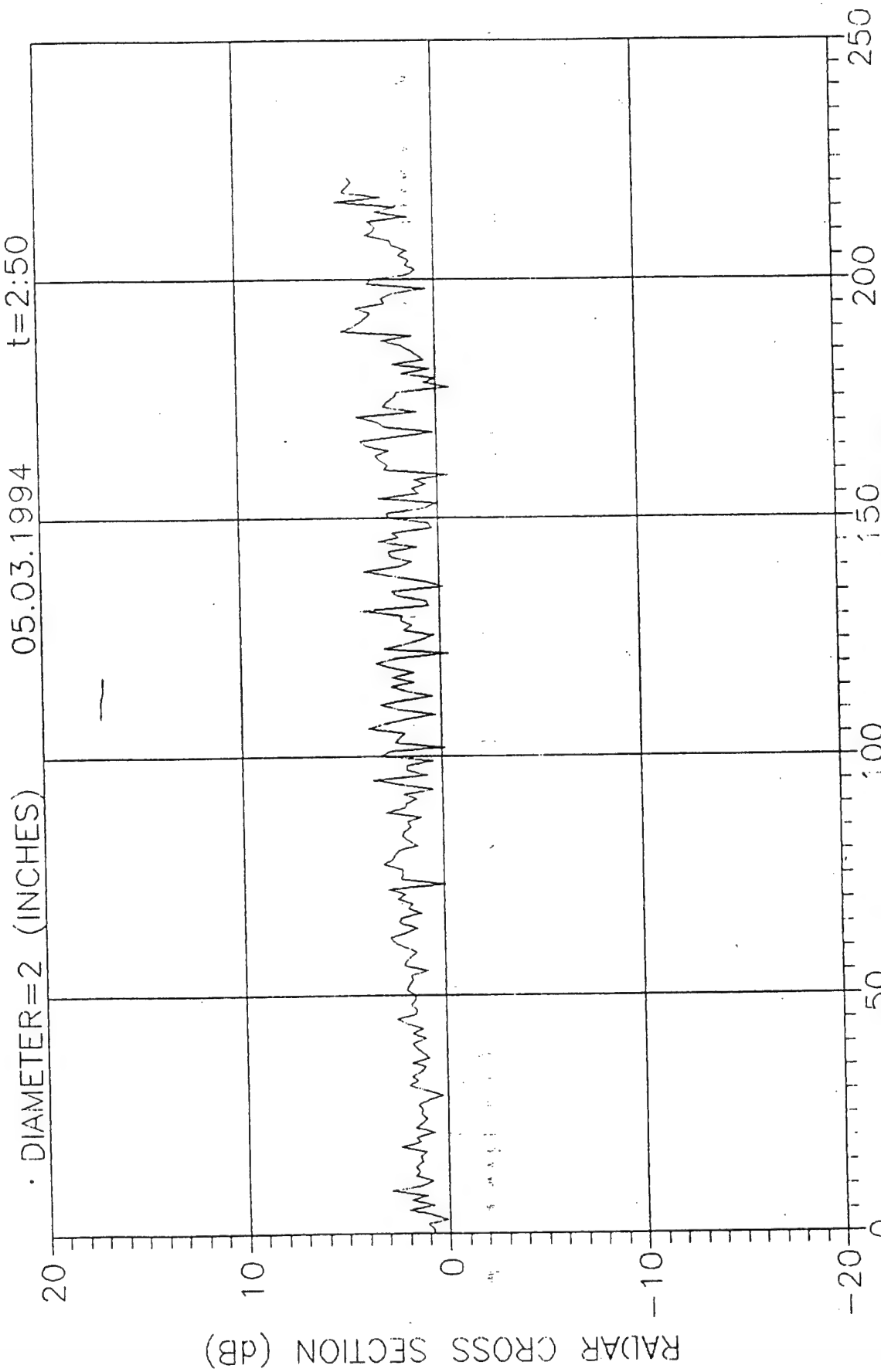

Fig. 1.2.8 Experimental RCS values

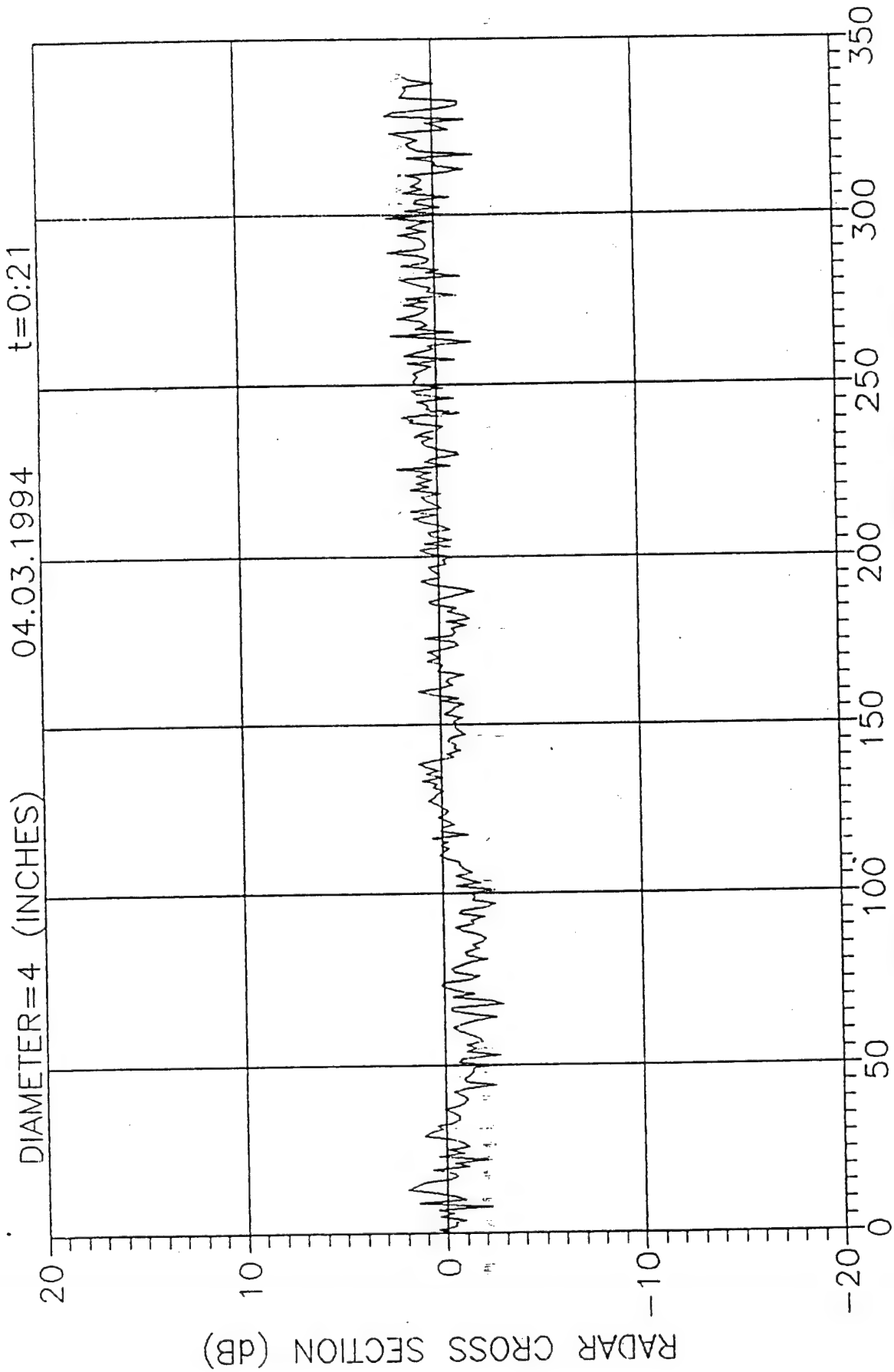

Fig. 1.2.9 Experimental RCS values

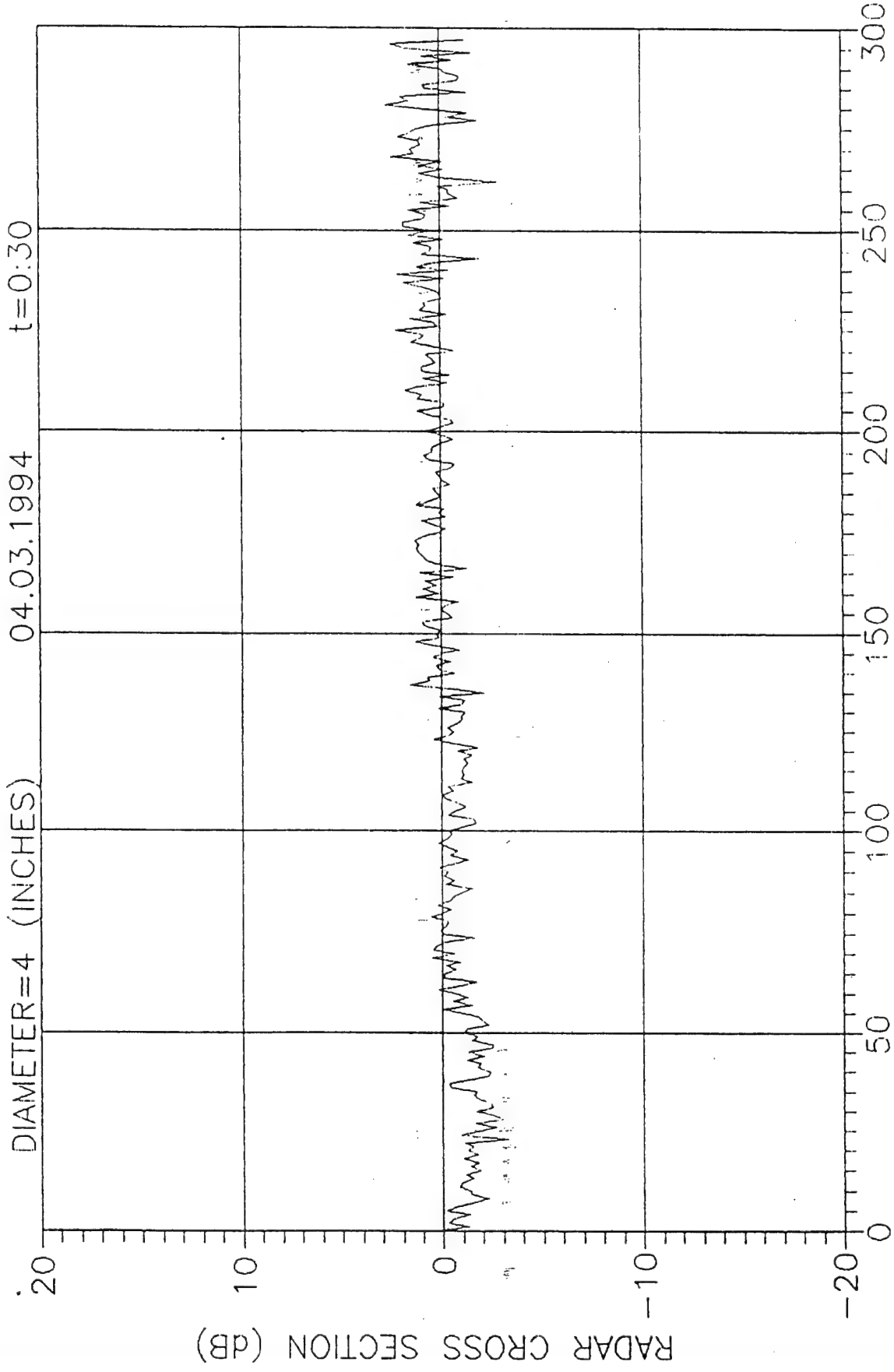

Fig. 1.2.10 Experimental RCS values

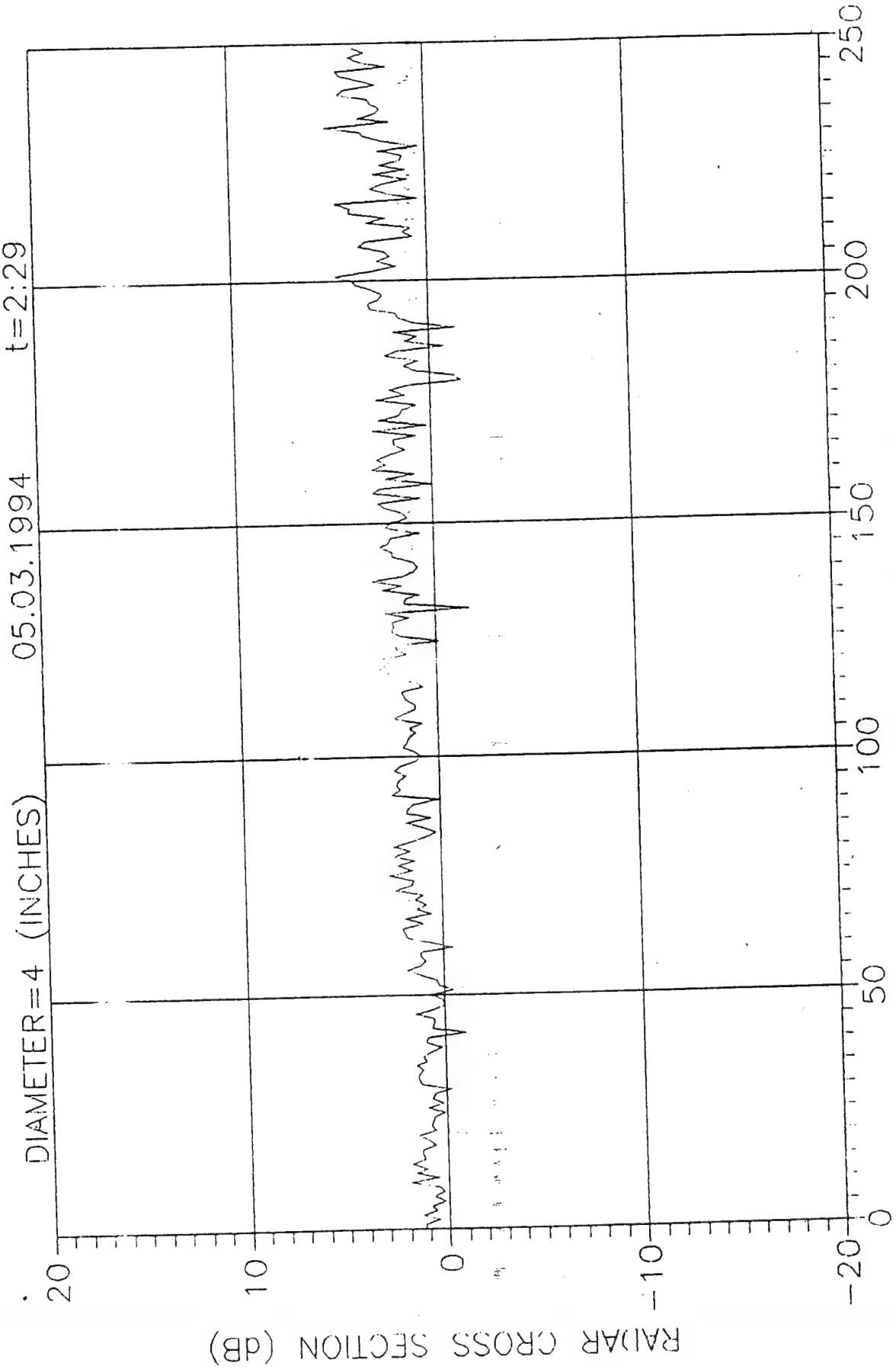

Fig. 1.2.11 Experimental RCS values

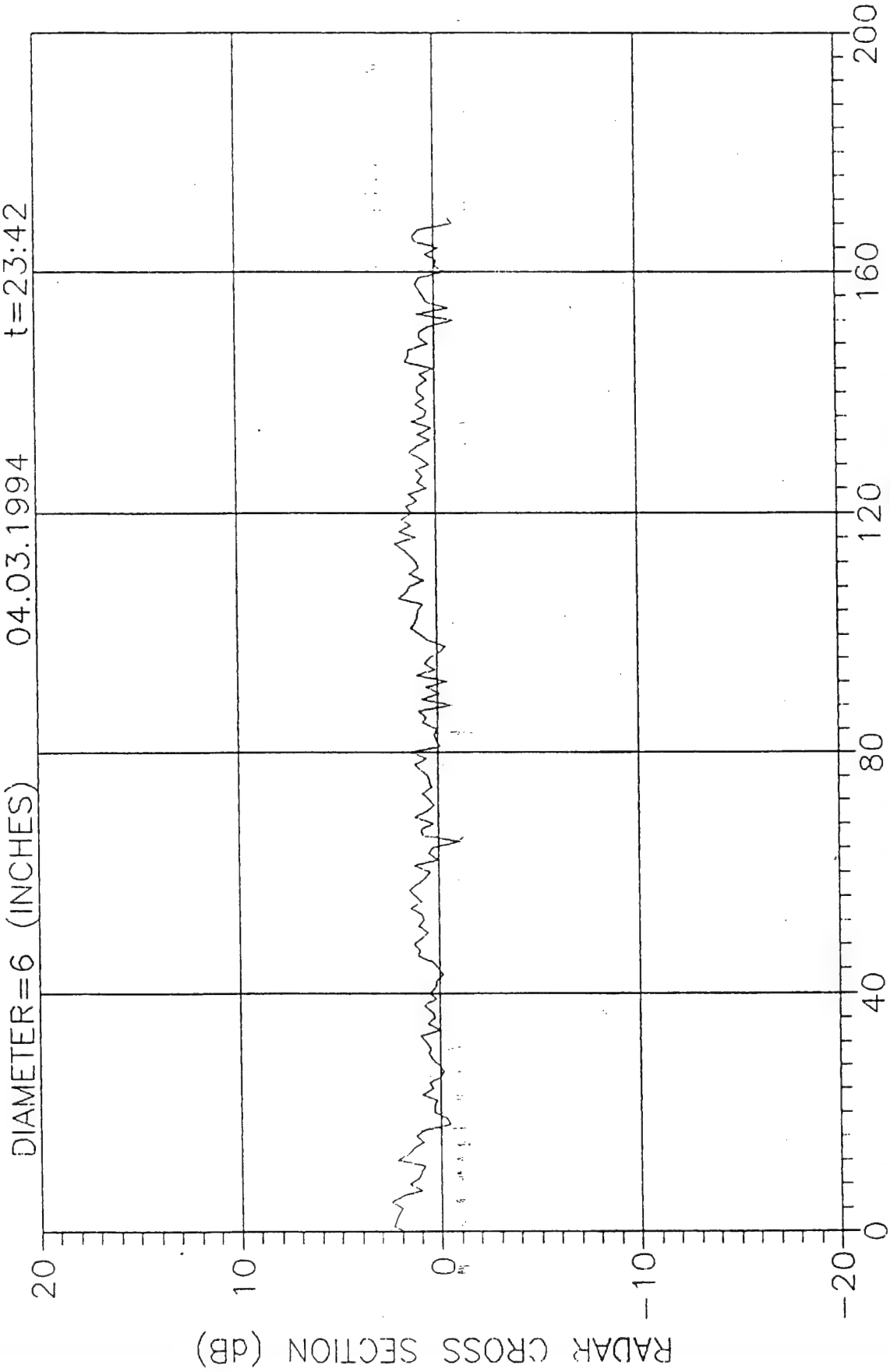

Fig. 1.2.12 Experimental RCS values

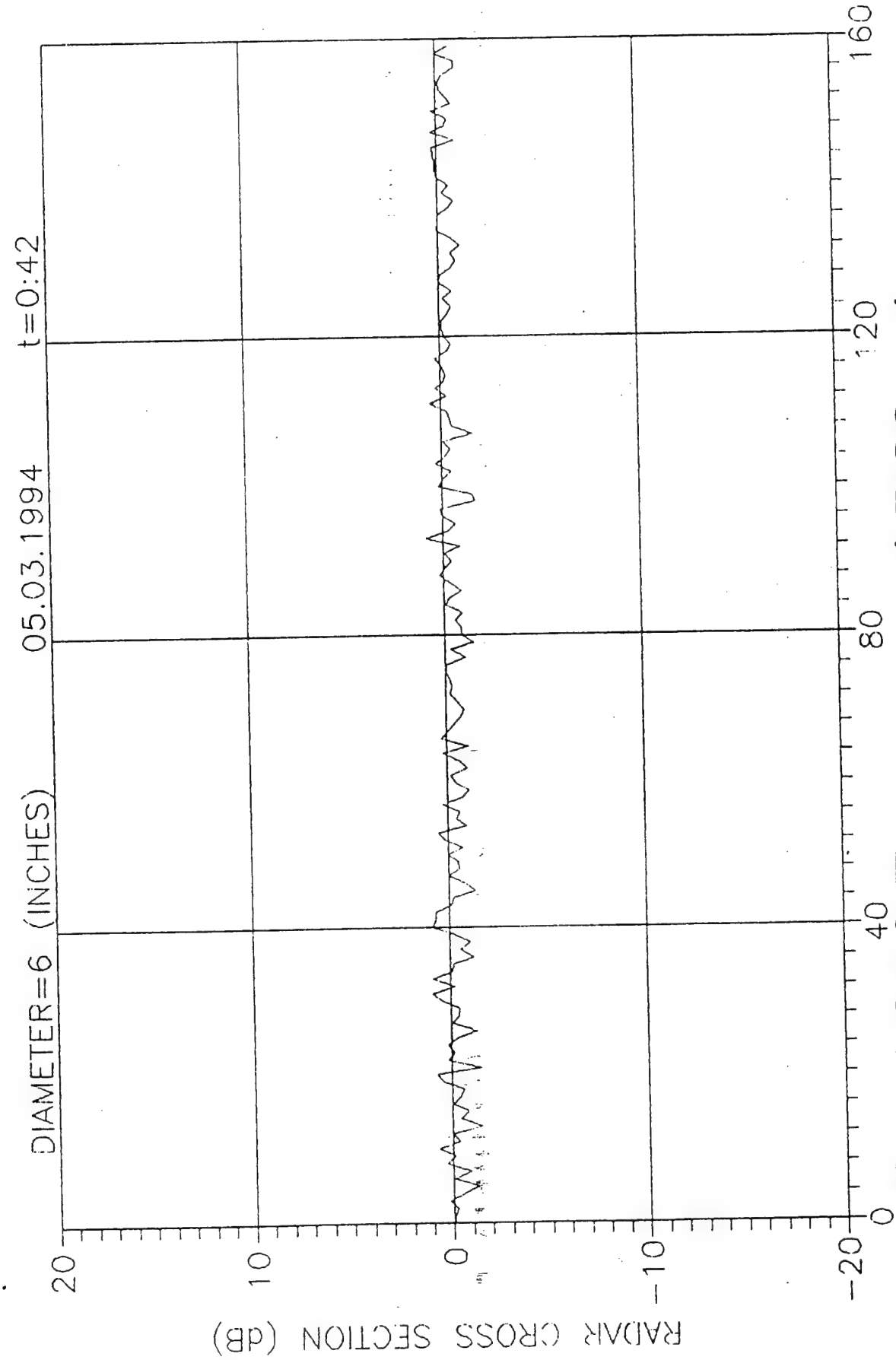

Fig. 1.2.13 Experimental RCS values

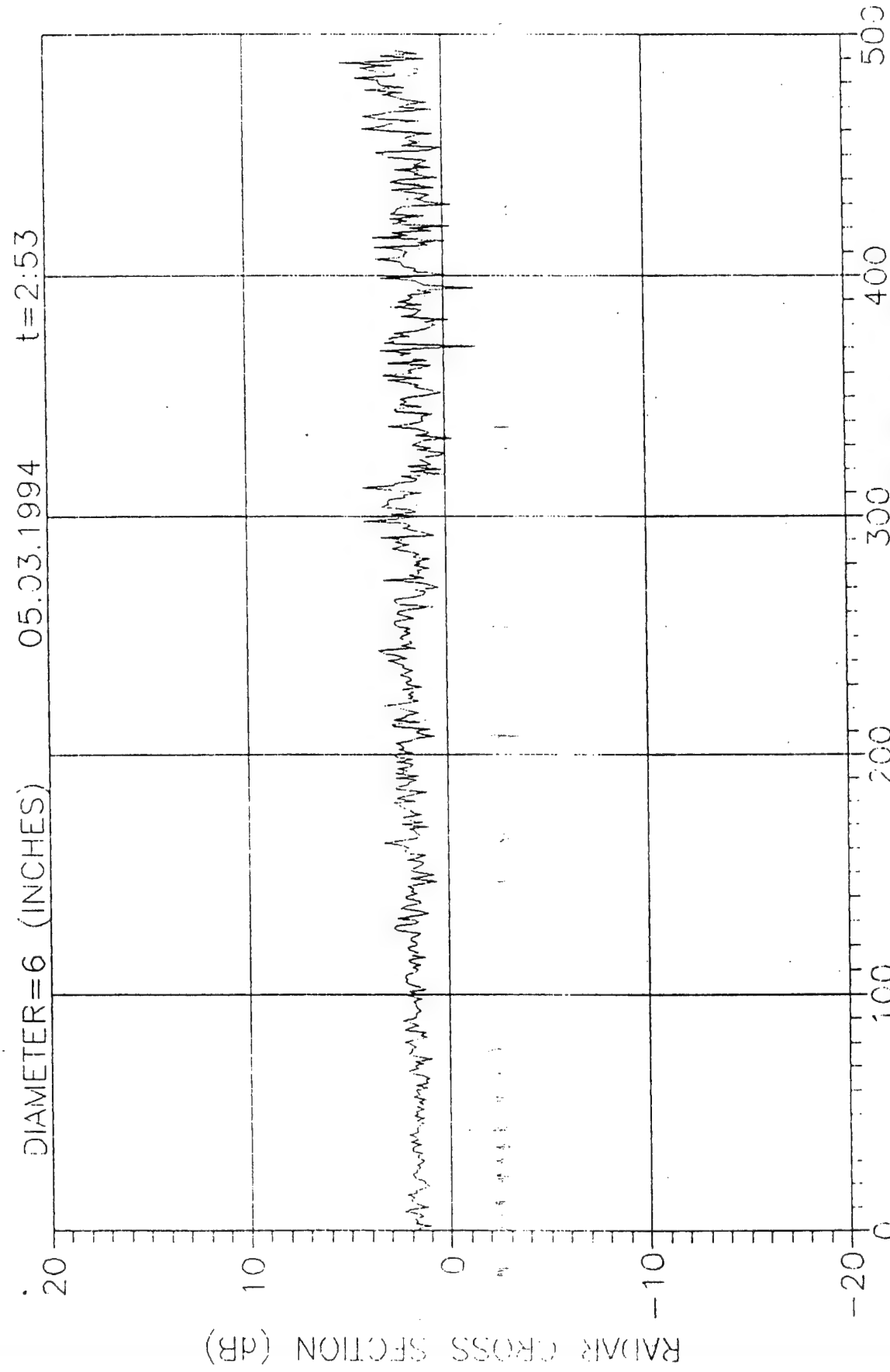

Fig. 1.2.14 Experimental RCS values

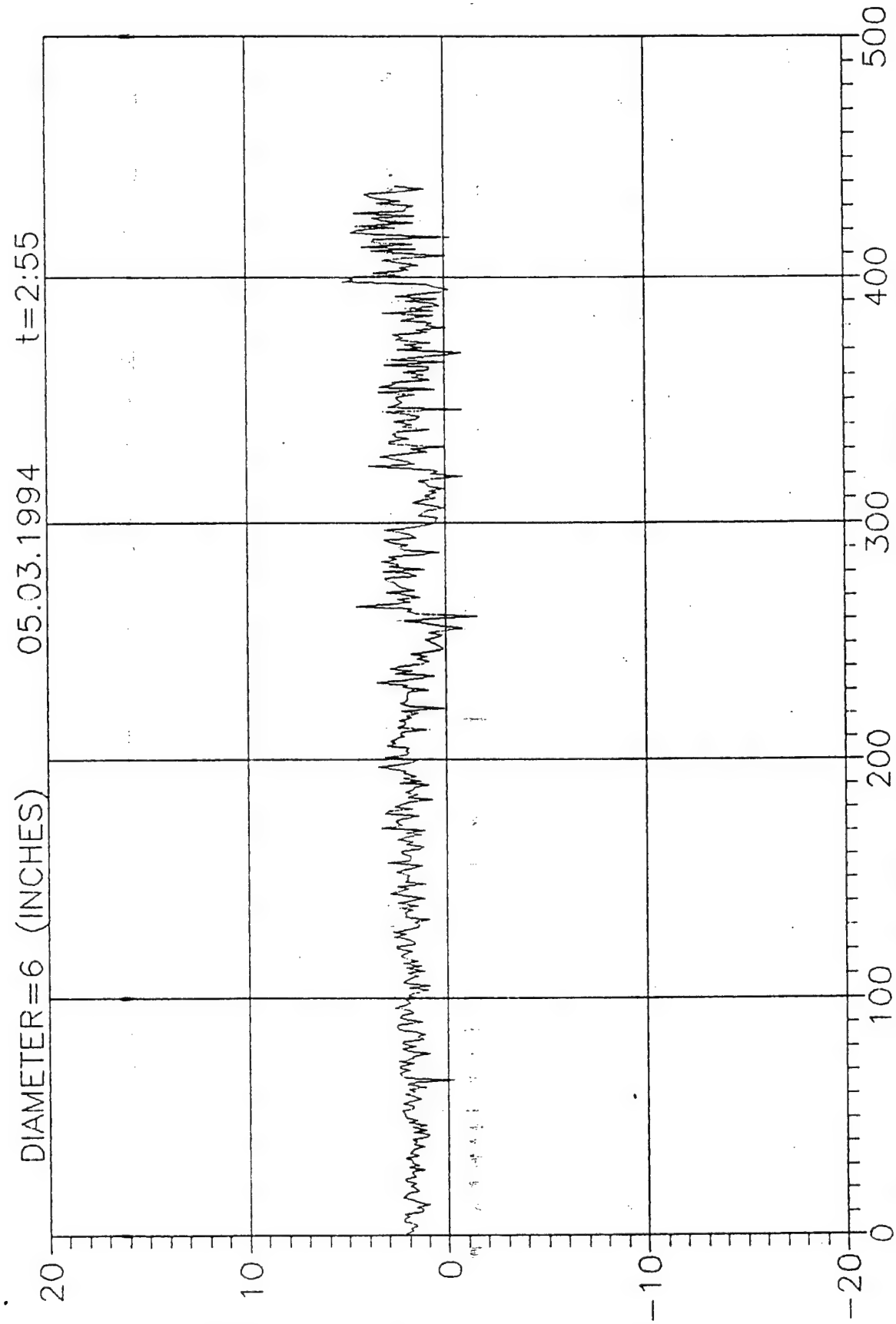

Fig. 1.2.15 Experimental RCS values

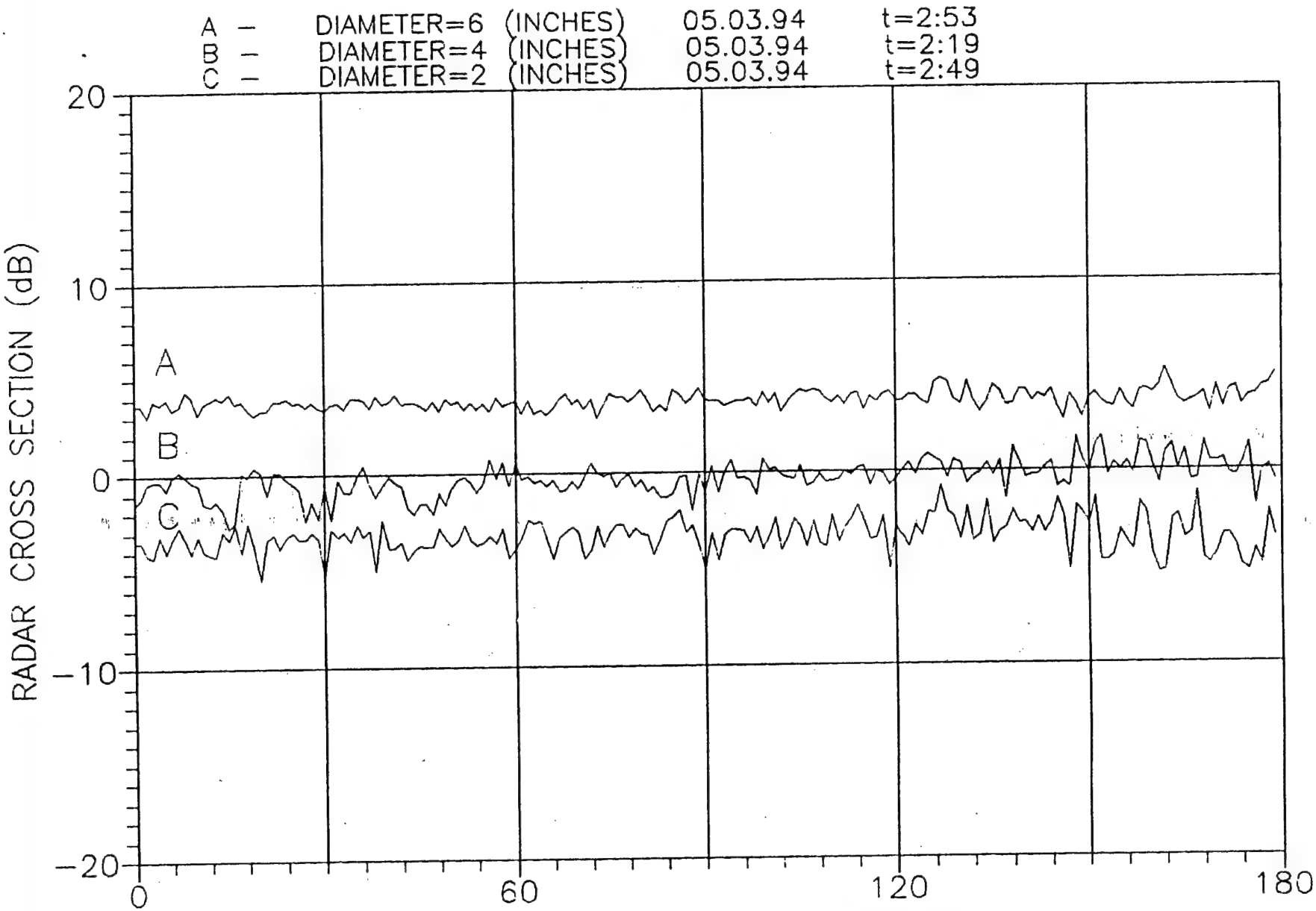

Fig. 1.2.16 Experimental RCS values

14 m - for metal asteroids (reflection index is 0.6).

To introduce this mode of operation it will be necessary to update considerably the radar software and to perform respective trials before the actual experiment.

1.3. Capabilities of dm-band radar's

BMD radar's operative in the short-wave segment of the dm-band.

These systems employ mechanical scanning of reflectors for search of objects in the upper hemisphere , plus electron scanning of a narrow beam within a limited volume. The radar's are located in the Moscow Region.

Fig. 1.3.1 presents the calculated radar detection range as function of the SO size.

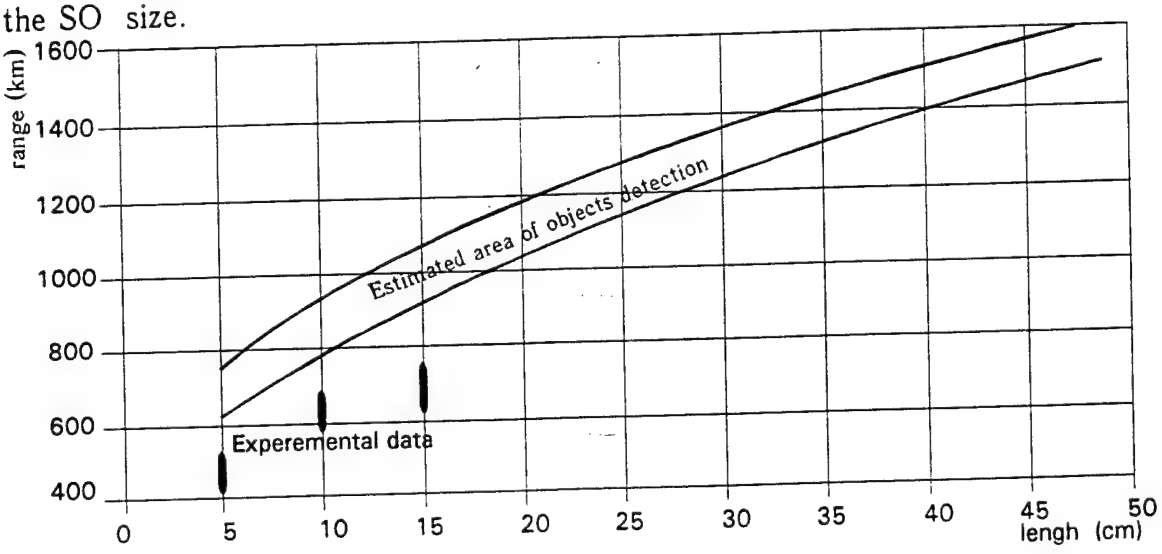

Fig. 1.3.1. Estimates and experimental data from the dm-band radar.

Experimental results are presented in the same figure. Three radar's spaced at distance of about 100 km from each other were used in the experiment. 27 observation sessions with duration of 3.5 min each have been carried out. The detection ranges registered in the experiment turned to be lower than the calculated ones. This is due to the fact, that the search zone was set up smaller, than that observed in the normal operations mode. The signal-to-noise ratios obtained in the observations were higher than the threshold levels, which confirms validity of the calculated curve for the normal operation mode of the radar's.

1.4. Capabilities of the mm/cm-bands radar complex

The experimental dual-band (cm & mm) radar complex is Located at a site near Lake Balkhash (Kazakhstan).

This dual-band radar complex includes two high-potential pulse radar's with steerable phase array antennas, which enable surveillance of objects in the upper hemisphere.

An assessment of the radar complex capabilities to detect orbiting space debris was done under the following assumptions:

1. The radar complex employs the following observations mode: beams of both radar's are pointed to a single area (e.g. to zenith). So a barrier is formed - as wide as possible, and surveillance of the near-Earth orbits is initiated. As soon as a space object is detected, surveillance mode is changed to the local area sounding mode. Procedure of sounding is optimised then.

2. The flow of space objects through the radar burrier is considered to be uniform.

3. Multitude of debris shapes is approximated into three metallic (aluminium of steel) geometric figures (cube, thin rod and thim discus) of various size.

Calculated dependencies of the radar-detected on the size of space objects re presented in Fig. 1.4.1.

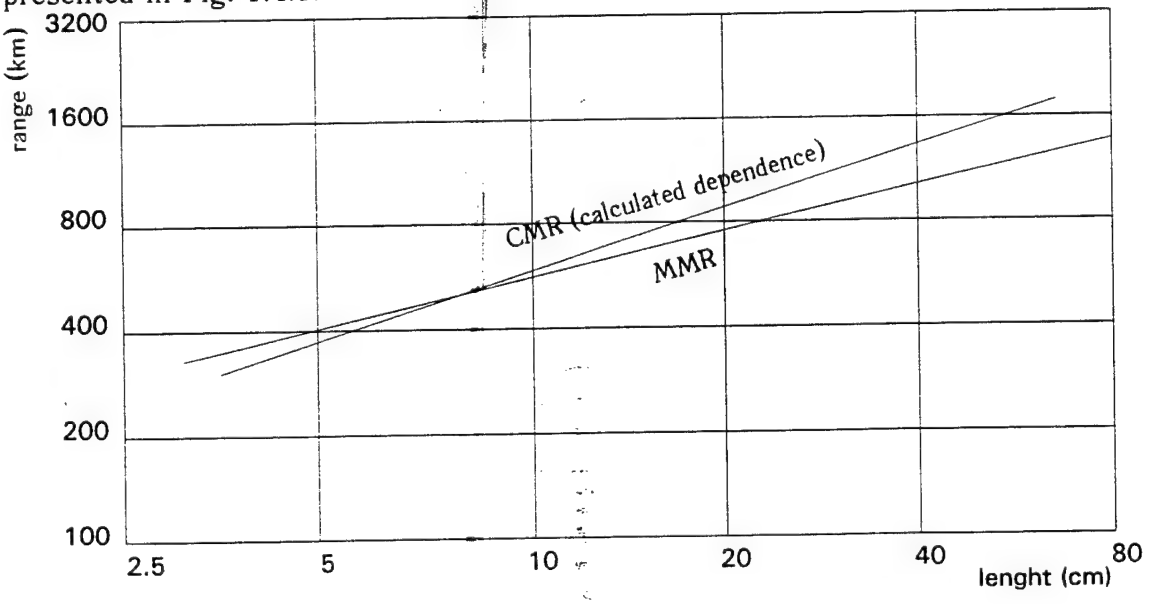

Fig. 1.4.1. Estimates of cm-band/dm-band radar complex capabilities.

Our calculations show that to assess characteristics of space debris in the upper hemisphere it will be necessary to perform 20 two-hour sessions with the cm-band radar (CMR) (to identify objects within the 500 to 1500 km layer) and some 400 two-hour sessions with the mm-band radar (MMR) (within 180 to 1000 km layer).

Chapter 2. Capabilities of Ground based Telescopes for Detection of Space Objects

2.1. Mobile multipurpose telescope

The medium- altitude orbit observations of space objects can be made using telescopes. The distance to the object can be calculated from interational data with the orbital parameters. Measurements of angular co-ordinates of detected object are required.

Two-point observation as shown on Fig 2.1.1 allow to obtain the distance to the object instantly after its detection. The most convenient second instrument for the so called "based observations" would be a mobile, multi-functional telescope under development now in Russia for space debris monitoring (see Fig. 2.1.2). Its characteristics: the Ritchey-Chretien telescope with the diameter of 60 cm and the focal distance of 3.6 m. The field of view is 20' with the resolution at the centre not worse than 1". The slew velocity is: by azimuth - up to 20 deg/s, by elevation - up to 6 deg/s.

Operation modes:

- detection of SOs with brightness up to 17 stellar magnitudes;
- position measurements with accuracy of 1";
- all kinds of non-positional measurements.

Light receiver:

a hybrid TV-system (Image Intensifier+CCD matrix) with the signal accumulation time up to 20 s, coupled with units of video-memory, signal digitalisation and computer interface.

Analysers:

- a set of colour filters for photometry in B, V, R-bands;
- slitless afocal spectrograph with dispersion of 5...75 nm/mm;
- polarimeter with capability of adaptation of object analysis modes to the brightness of objects.

Photometer:

automated tracking electrophotometer with a pulsating field diaphragm. Measurements are done by the method of photons counting in the integral light flow.

Application of an array of such telescopes makes it possible to overlap a poorly monitored medium- altitude zone (5 to 25 thousand km); to obtain

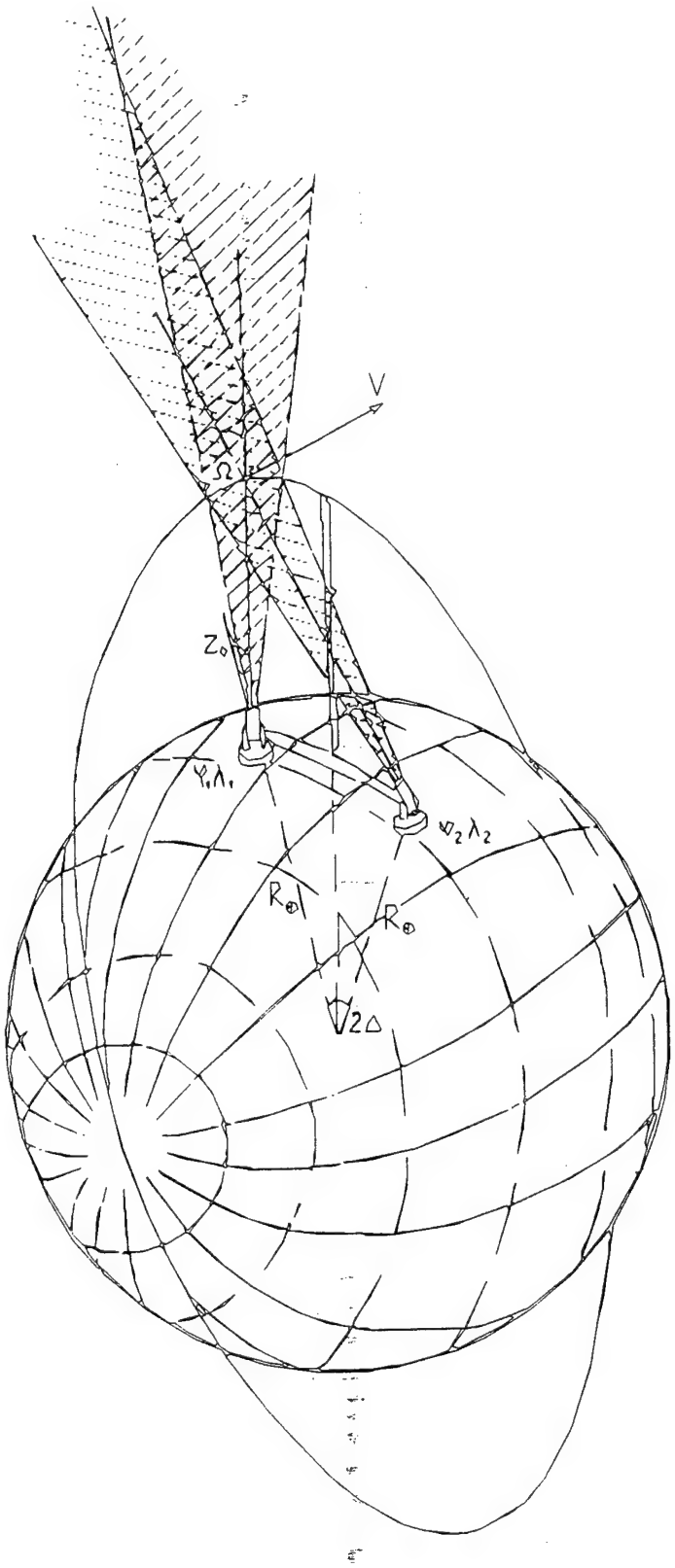

Fig. 2.1.1. A scheme for basis observation by two telescopes.

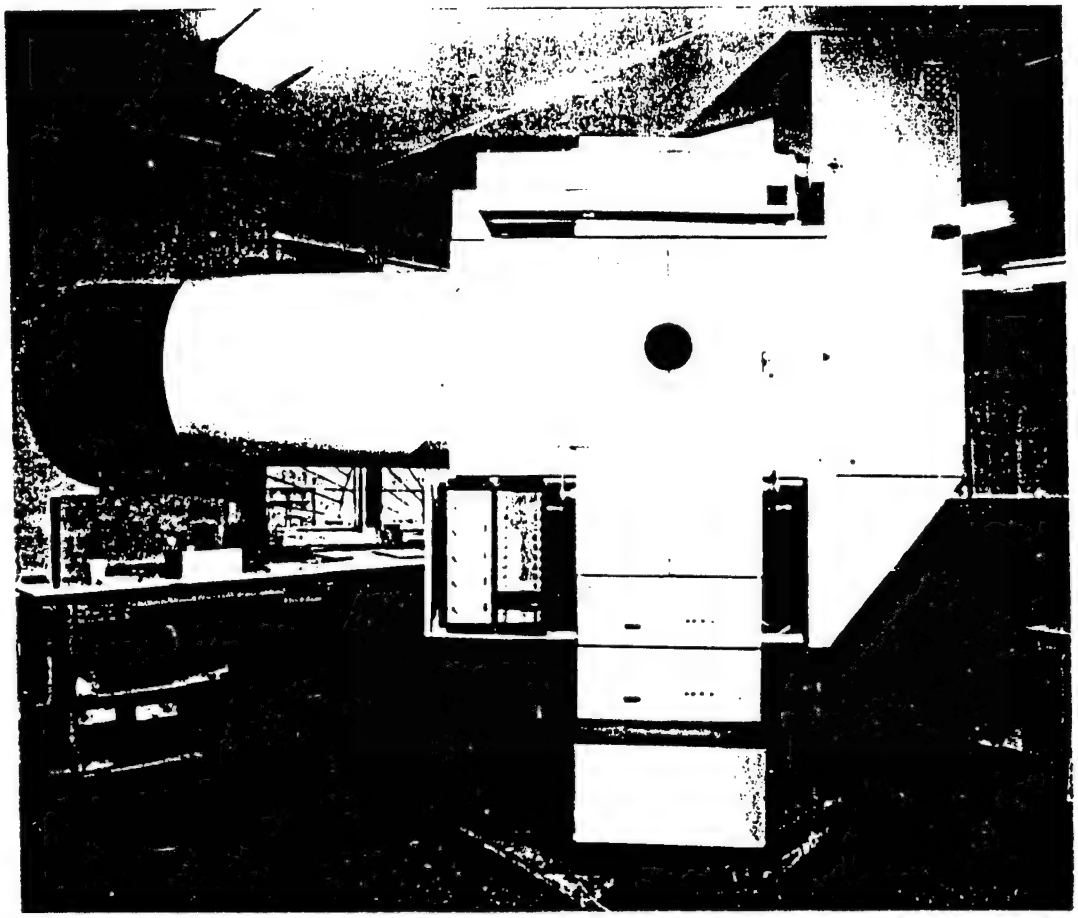

Fig. 2.1.2. Mobile multipurpose telescope

information on dielectric debris, as well as data on physical properties of objects by results of photometry, spectrometric and polarisation observations , along with simultaneous co-ordinate measurements.

There exits design documentation for the system, its primary elements have been tested out and patented. An existing Russian mobile lidar is taken as baseline system.

Light-reception sensors and respective software were developed and verified at the Simeiz and Zvenigorod astronomy observatories during observations of geostationary objects.

Results obtained from single channel electrofotometer sith pulse-type diafragm showed that using it the observer can identify SC shape and it individual elements, even when highest magnification of the telescope the SC is seen ad a dot.

Employment of afocal slitless spectrograph revealed its capacity to identify type of materials used in construction of the SC elements.

A unique spectropolarimeter for studies of polarisation characteristics of SC is on trial snow at the Simeiz. Observatory Baseline observations of GSCs confirmed that they have Nigh information content in particular it is possibly to separate diffuse and specular components of reflected light.

Estimated cost of a single optical monitoring station is 1.5 ... 2.5 million USD.

In the initial phase it is enough to have there 2 - 3 instruments, and then add new instruments when necessary.

2.2. Hybrid opto-television sensor

The task of observation of objects in the geostationary orbit (especially of the non-controlled objects) has its specific features. Due to the fact that motion of non-controlled objects has librational character, it is necessary to observe them during an extended period of time (some 300 - 500 days) to identify them reliably. Therefore, of great importance here is the use of non-coordinate information (photometric, spectral and polarimetric data). It enables us to perform rapid identification of objects, to make assessments of their shape, orientation, reflectance properties of the surface, to register their manoeuvres, to make accurate forecasts of motion for descending objects etc.

Positioned and photometric observations of space objects can be performed by the hybrid opto-television sensor, deployed at the Simeiz Observatory (Crimea). It employs a one-meter telescope with the maximum permeating capability - 17.46 stellar magnitude (in the integral light), and the dynamic range of the TV receiver of - 5 stellar magnitude.

Actual capabilities of the sensor were demonstrated during photometric observations of the TITAN-3/TRANSTAGE 13 spacecraft (object 68081E), which broke up in 1992. There were taken 35,265 measurements of brightness of the object. Brightness curves had the duration from 30 min to 5 hours. By the information obtained it is possible to solve the reverse photometric task - to reconstruct the shape of the observed object.

Chapter 3.
Capabilities of Space-based UV/Visible Sensors for Space Debris Observations

3.1. Russian UV- and visible-range sensors applicable for observations of small space debris fractions

There are three major lines in current research and development activities on the UV and visible bands sensors, applicable for observations of small-size fractions of space debris (SFSD) which include widely different objects - from clouds of technogenic particles with the size of several tens of microns to individual fragments with the size from 0.1 to 10 cm.

1. UV sensors (0.01 - 0.18 microns) on the basis of a *CsJ* photo receiver array. The photo receiver includes 800 × 800 elements, with the size of the light sensitive element of 23 microns, the quantum efficiency of ≈ 0.27, and the 8 MHz frequency of scanning.

2. There exists a more advanced design - the UV/Visible sensor on the basis of the micro channel plates (MCP) which is being developed specifically for the surveillance over individual fragments of small space debris. This sensor can be most adequately used for observations of small space debris in the UV and Visible bands due to its high sensitivity (≈ 10^{-17} J/dement) and smaller pixel size (≈ 15 - 12 microns), to practically total absence of inherent noise over the whole surface of the photoreceiving device, and because of its capacity to registrate individual photons and the time of their arrival. Small-size low-contrast objects moving in space can be detected thanks to such measures as coupling of the photoreceptor device with a high-capacity transputer-based onboard computer, employment of co-ordinate and temporal registration of the photo current, use of conveyor-type computation in the initial phase of data processing, and application of special-purpose algorithms for identification of the useful signal.

Micro channel plates - based photo receiving devices are able to operate without cooling both in the UV and the Visible bands, which is a very important feature enabling us to use them for space borne observations of small fractions of space debris. It is planned to complete in 1994 activities on ground-based experimental verification of the sensor hardware and software.

3. UV gas-discharge chambers can also be employed for observations of solid rocket motors effluents and other clouds of micron-size techogenic particles which pollute the near-Earth space environment. There are such specific features in this type of sensor as employment of the multi-channel plate in the photoreceiming device, along with the CCD-array and interferention filters.

Schematic diagram of the MCP-based sensor is given in Fig. 3.1.1.

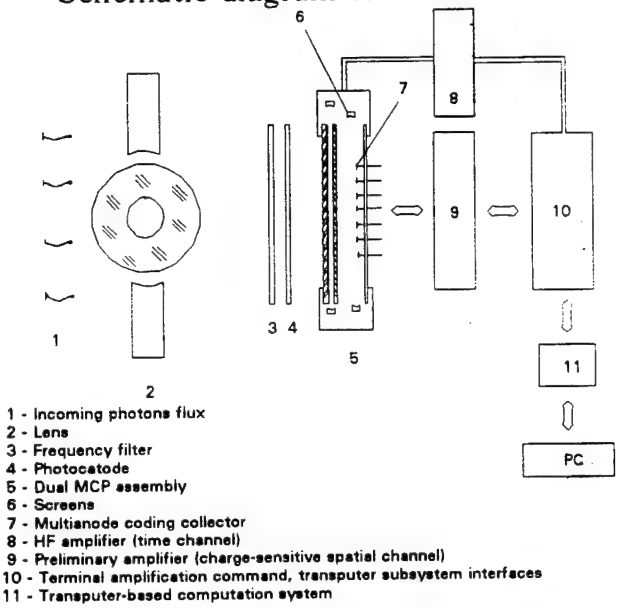

Fig. 3.1.1. Schematic diagram of the MCP sensor.

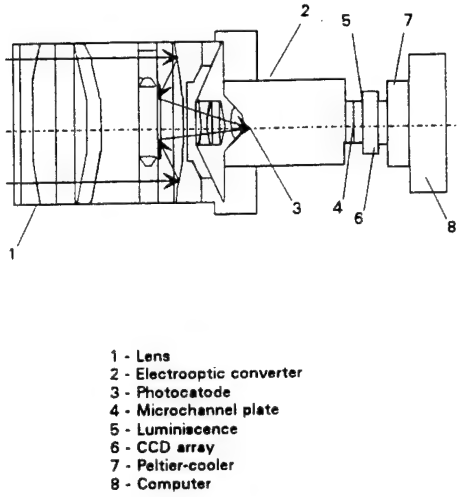

Fig. 3.1.2. Layout of the UV chamber

For the MCP-based sensor There was developed a laboratory prototype that is used for tests of hardware and checkout of software. To observe SSDF fragments larger than 0.5 cm in size at the distance of 100 km a special instrument is under development now. This device has an input pupil diameter of about 5 cm, the focal length of about 50 cm, size (diameter × length) of 10 × 50 cm approximately, power consumption of about 5 watts and mass close to 3 kg. Its field of view is 0.02 radians.

Algorithms developed for information processing represents a successive fulfilment of four processing stages with preliminary data accumulation during some tine interval T (see Fig. 3.1.3). At the first stage the data flow is initially ("roughly") purified from elements corresponding to background photons. Since the three-dimensional space (x, y, t) regions corresponding to object's trajectories are filled with (x_i, y_i, t_i) points $(1+a)$ times thicker, than the remaining part, only

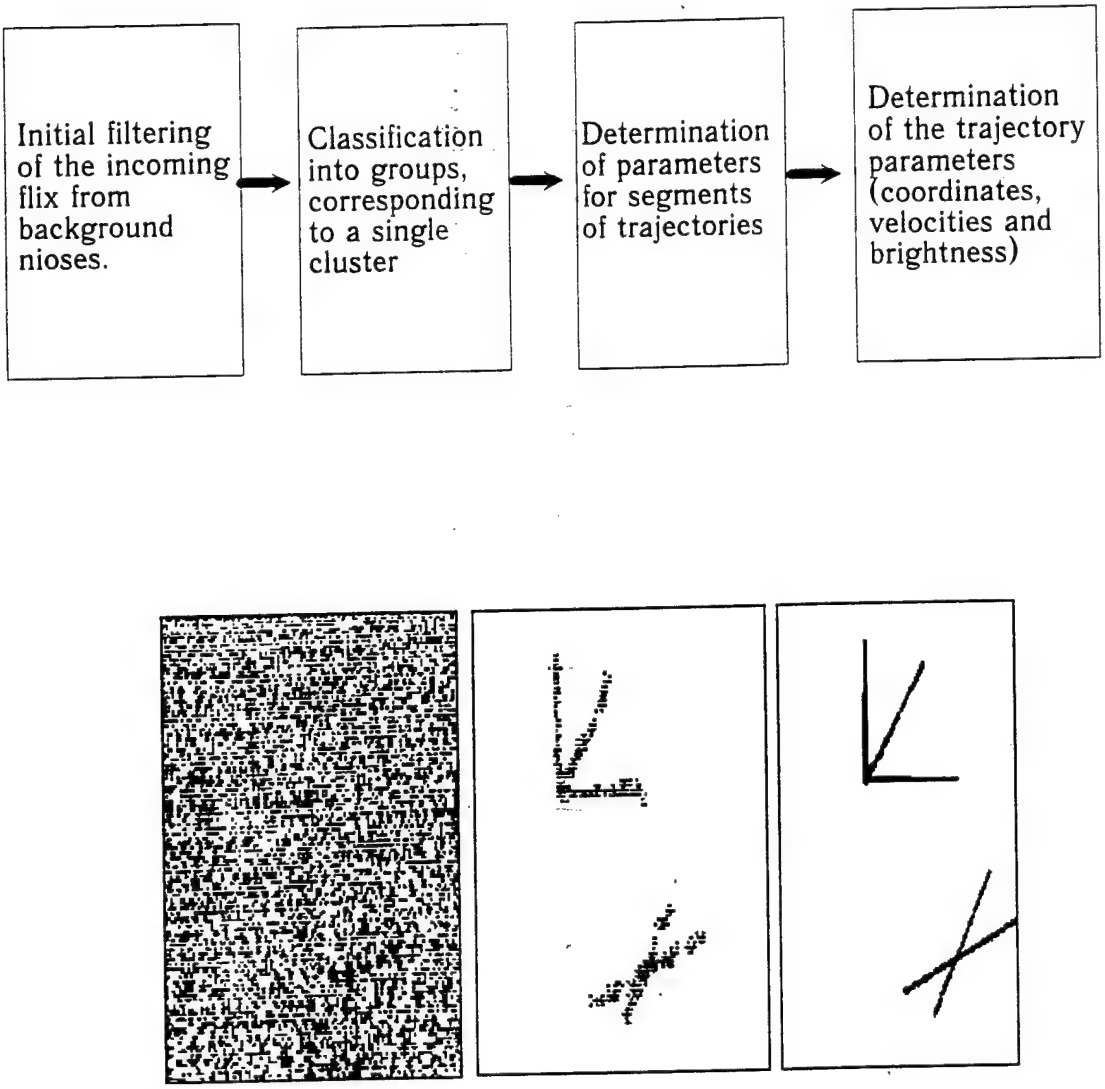

Fig. 3.1.3. Diagram of the algorithm and an example of its application.

those (x_i', y_i', t_i') "threes" come to the first stage output, which are fallen into thickening regions. Here quantity a is the signal-to-noise ratio.

At the second stage remaining "threes" are divided into groups, each of which corresponds to one thickening region. Too small groups are disregarded.

At the third stage the decision is made for each group: are there any fragments of trajectories in the group and how much. If yes, the final purification is done and the parameters of trajectory of fragments are determined.

At the fourth stage the complete trajectories are composed from the fragments obtained, and their parameters (such as co-ordinates, velocity, brightness) are found. The laborious-ness of the fourth stage is negligible compared to the preceding one.

Fig. 3.1.3 gives an example of program implementation of the algorithm of C language for IBM PC. Three rectangles depict a a focal plane. The left rectangle shows the map of recording the input flow of photons; the middle rectangle demonstrates the background; the upper rectangle shows the superposition of true and found trajectories.

Preliminary evaluations of possibilities to observe the SSDF were done using a Russian model of assessment and forecast for the degree of pollution of the near-Earth space (Prof. A.I.Nazarenko of the Centre for Program Studies is the author of this model).

Evaluations given in Table 3.1.1. were prepared with using a sensor having the observation angle of about 0.02, which makes it possible to detect a 0.5 cm fragment at the distance of 100 km from the orbital station MIR (the orbit altitude is 350 km, inclination is 51 deg) with due account of possibility of observing the fragments of the sunlit side of the Earth.

Table 3.1.1.

Object size, cm	0.5...1.0	1.0...3.0	3.0...6.0	6.0...10.0	10.0...30.0	> 30.0
Number of objects observed per one orbit	10...20	2...4	0.1...0.2	0.1...0.2	0.15...0.4	0.1...0.2
. Number of objects observed per one min.	0.1...0.2	0.02...0.04	0.001...0.002	0.001...0.002	0.0015...0.004	0.001...0.002

The Table indicates that the flow of observed SSDF makes no great difficulty for data processing operations. The relative time for observing at least one object in the MIR vicinity comprises about 30 % of the total observation time. The size distribution for of simultaneously observed objects larger than 1 cm is as follows:

1 object about 90 %
2 objects about 9 %
3 and more objects about 1 %

The second instrument - the UFK ultraviolet camera - has already been used in orbit during the 14th expedition to MIR in late 1993 - early 1994. This camera was employed for observing the Earth background, Earth limb, PROGRESS cargo and effluents from its rocket threshers during approach to, docking and unlocking with the orbital station. A spectral feature of the filter was its suppression of background from the visible spectral region. The investigations were carried out with a photo camera using UV-optics and recorded on a film sensitive in the UV-range. The observation results have been analysed. The UFK camera characteristics are indicated in Table 3.1.2.

Table 3.1.2.

1.	Objective-mirror and lens: Aperture, mm D/F radio Effective diameter of the entry bore, mm Wavelength band, nm Field of view, deg	 73 1 : 1 53 200...300 12
2.	Image intensifier: Window Photo cathode Spectral band, nm Amplification	 MgF_2 Cs_2Te 110...320 $30...3 \cdot 10^4$
3.	CCD matrix: Number of pixels Pixel size, μm	 760 × 580 24 × 32
4.	Full dynamic range	$> 10^5$
5.	Exposure time, sec	0,01...10
6.	Sensitivity, watt/cm.^{2} sterad.A	$2 \cdot 10^{-14}$
7.	Dimensions: Diameter, mm Length, mm	 120 300
8.	Mass, kg	2,5

3.2. Application experiments whis space- based sensors

Space borne experiments with various space-based sensors have been carried out by Russia over 20 years. In particular, following sensors were flown:

- UV-band instruments developed by Russia, Germany, Chechoslovakia and other countries and used in 1970s - 1980s in a series of experiments for investigations of the solar activity and its influence on the upper layers of the atmosphere, within the framework of the INTERKOSMOS and VERTIKAL programs (over 10 flight experiments);

- the 80 cm telescope on board the ASTRON spacecraft used for observation of stars, composition of the upper atmosphere of the Earth, and the Halley comet during 1985-1992;

- a modified variant of the telescope TEREK-K is planned to be installed on board the KORONAS-N spacecraft to be launched in 1994 (see Fig. 3.2.1). This telescope has a higher resolution (up to 2 arc.sec), a matrix image receiver with the number of elements of 760 x 580 and an advanced model of the coronograph, in which the dissipated light level is reduced the 10^{-9} of the incoming flux; the sensor has additional channels in the spectral area of >1000 A for investigations of the upper atmosphere by observation of the Sun at the limb. Direct observations of the atmosphere on the shadow side of the Earth will be conducted in the UV band also. We plan to incorporate into the results of this experiment the new data on absorption and diffusion of UV emission in the Earth atmosphere at altitudes of 50-300 km with the resolution up to 1 km in altitude and also the data on the intristic UV emission of the Earth atmosphere. This sensor can be used for observations of clouds of technogenic particles, which pollute the near-Earth orbits.

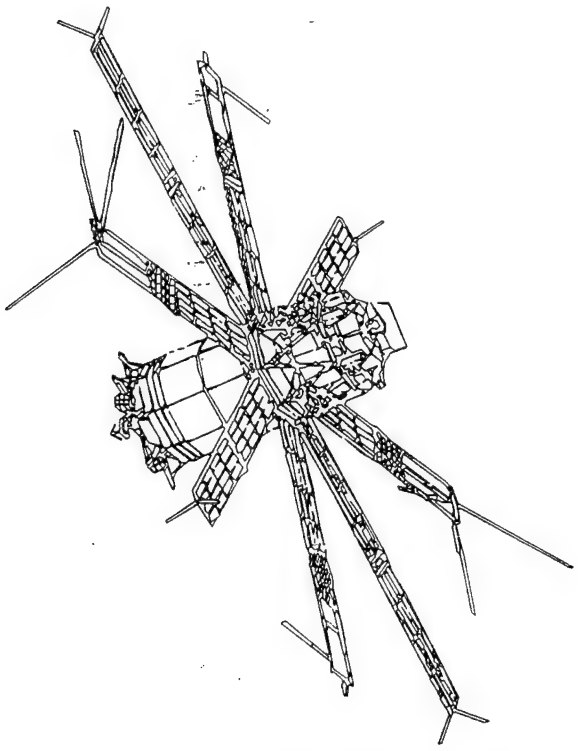

Fig.3.2.1. The KORONAS spacecraft.

Experiments in which the UV and visible-band optoelectronic sensors are carried out at the MIR station (see Table 3.2.2).

Table 3.2.2

Characteristics	Value
Spectral band, mcm	0.2 ... 0.34
Pixel diameter of the optics, mcm	0.5
Pixel diameter of the photodetector unit, mcm	11
Sensitivity threshold of the photodetector element, J/sq.cm	10^{-10}
Threshold quantity of photons pixel	120
Background noise per pixel	$5 \cdot 10^{-3}$
Period of the interframe subtraction, sec	110

The most favourable situation exists now with sensors operating in the visible and near IR spectral bands (0.4...1.1 mcm).

Photo receivers with the format of 521 × 521 to 4096 × 4096 elements were manufactured or being developed now. Their sensitivity equals to $10^{-10}...5 \cdot 10^{-12}$ J/sq.cm (i.e. $10^{-11}...10^{-12}$ J/pixel), which is close to the physical limit.

Table 3.2.3 presents parameters of some visible-band and near IR-band sensors.

Table 3.2.3

Basic parameters	NII "Pulsar"	NPO "Electron"
Array parameters:		
Number of elements in an array	2048 x 2048	2048 x 2048
Photosensitive element size, mcm	24 x 21	24 x 21
Operation wave band, mcm	0.4 x 1.1	0.5 x 0.8
Threshold sensitivity, J/sq.cm	10^{-10}	$17 \cdot 10^{-10}$
Array elements in the time delay and filling mode:		
Operational spectral wave band, mcm	0.4...1.1	-
Number of elements in the array	2048 x 2048	-
Photosensitive element size, mcm	16 x 12	-
Threshold sensitivity, J/sq.cm	10^{-10}	-

Optoelectronic devices operating in the visible and IR-bands are used on board the EKOL and MONITOR spacecraft (SC) developed for ecological monitoring. Multispectral scanners of low, medium and high resolution in the visible and IR-bands are installed and used on-board the RESURS F and RESURS 01 SC for remote sensing of the Earth.

There also exist multispectral stereo TV cameras and video spectrometers, which can be readily applied for the SSDF surveillance purposes.

Chapter 4.
Capabilities of Ground based Radar's and Telescopes for Detection of Asteroids

Recently an interest to the astronomical aspects of the "Asteroid hazard" (collision to the Earth) has increased. It is known that the collision of the asteroid larger than 2 km with the Earth will cause (is equal) to the global catastrophe [4.1]. But it is also known that the probability of such event is rather low.

The astronomers have studied well the main population of the asteroid bodies of the Solar system. As for the meteoroids, there is a complete information about them with the sizes less than a few centimetres [4.2]. But the meteoroids with sizes of few centimetres up to hundreds of meters, which are mostly dangerous, are not studied. The task can be stated as following: to estimate the possibility of the observation in the meteor streams of asteroids and meteoroids with sizes from few centimetres up to hundreds meters in diameter. Is it possible to carry out such observations using modern radar and optical facilities? Let us consider this task in details.

We are of the opinion that solution of the given problem will require to employ both existing optical telescopes, and cm-band BMD radar described in Section 1.2 of our Report. We take into account that the radar's use a special mode with accumulation up to 100 return signals and also employ a narrow-beam mode of operation with external target designation. Therefore, the radar's capabilities for detection of space objects correspond to the calculated one and they are given in Fig. 1.2.17.

Capabilities and the technique for conducting of the experiment can outlined as follows:

- Detection of an Earth-bound asteroid with the size of 10 m is done by optical telescopes at a long distance.
- Information from optical sensors is used for computation of trajectory data on the detected celestial body, and they are fed as target designation inputs to the radar. The latter performs detection of the Earth-bound asteroid at a shorter distance.

Requirements to the optical sensors regarding the accuracy of target designation inputs:

- velocity $\pm$ 1 km/sec;

- distance ≤ 650 km;
- angular co-ordinates ≤ 2 + 2 deg.

The detection of asteroids small at trajectories of collision with the Earth comes to the detection of objects in the vicinity of the Earth that have low or zero apparent angular velocity.

For the collision of space object with the Earth it is necessary that their orbital movements were compensated, i.e. multiplication of the difference between tangential components of their helio-central velocities by the time for closing in has to be not more than the Earth diameter (Fig. 4.1).

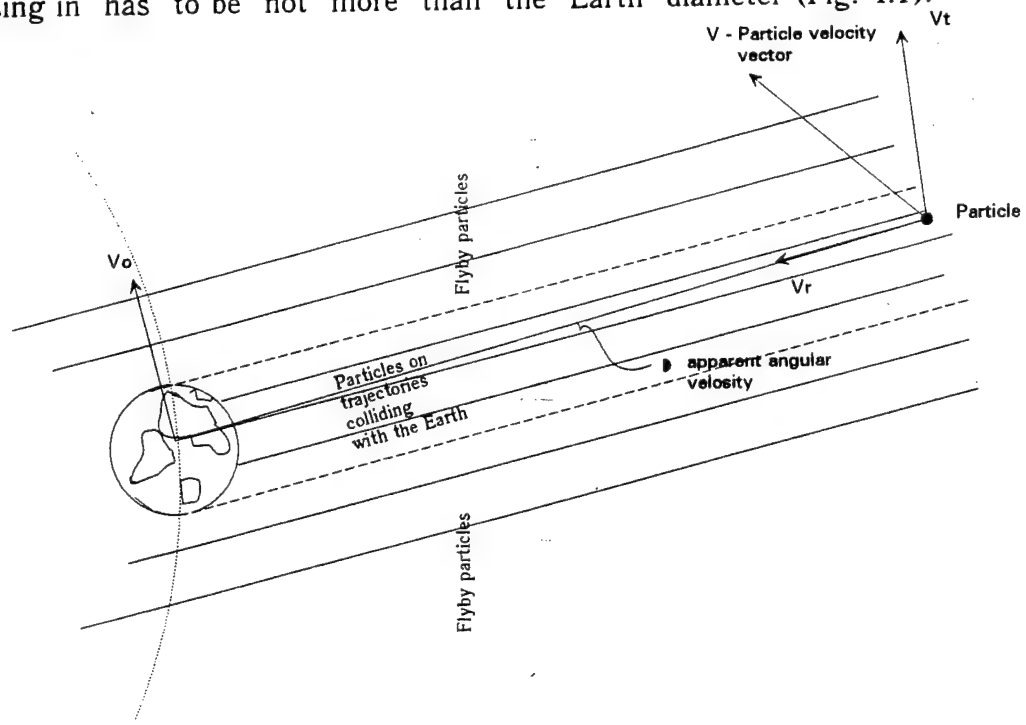

Fig. 4.1. Conditions of collision of meteoroids with the Earth.

In case of long-range detection - at least some hours before collision - the speed of closing in about 10 km/s leads for the distance to the board of detection zone to be 150...200 thousand km from the Earth. Obviously the lowest angle velocity will be when the object moves along the Earth orbit, and the largest one will be when the object is on traverse of the Earth. In the first case the visible angular velocity will be close to zero, and in the second - it will not exeed 2"/s.

A problem of the detection of "state" astronomical objects by means of various light detectors is now well-studied and discussed in publications [4.1,4.2].

A possible exposure time for detection of space object as a point-like one increases with the distance to the object (because of decreasing of its visible angular velocity). On the other hand if during the exposure time the length of the track exeeds diameter of an image of state point-like object, the detectivity power decreases as ratio of areas of their images.

An average seeing for astronomical observatories is 2" and does not depend of optical instrument. Taking in account that mean angular velocity of target object is 1"/s, it means that limit stellar magnitude at the optical space object detection will be achieved at exposure time 2 sec. As the brightness of object decreases as the second power with the distance, and possible exposure time increase only as first power of the distance (as visible angular velocity does), the most detective power of any optical instrument for this long-rage detection will be realised at time-exposure 2 sec.

Let us consider the meteor stream observations by a single observer on the Earth. The amount of meteoroids with sizes larger than d which can be observed is [pieces/hour]:

$$\Phi = (H.R) \cdot (S / S_0) \cdot [N(d) / N(d_o)], \qquad (1)$$

where: (H.R.) - the average number of meteors in the meteor stream, registrated by a single observer per hour;

S_0 - the effective square of the surface, observed by a single observer.

d_0- minimum size of the meteorite body, setting off the observed meteor (d_0=0.5 - 1 cm).

$N(d)$ - the relative amount of bodies with sizes larger or equal to d.

S - square, through which the particles with a registrated diameters larger or equal d will pass, and equal $S = \pi \cdot r^2$, and r [km] is related to d [cm] like:

$$d = r^2 / 16 \cdot 10^5 \qquad (2)$$

According to [4.2], the value of (H.R.) varies from 6 to 50 for different streams. (It should be noted that these values are obtained for the usual but not the anomaly years).

The estimation of S_0 is 3000 km^2. Using the r.m.s. approximation for the table of function N(d) from [4.2] we obtained:

$$N(d) = 4 \cdot 10^{-24} / d^{2.8} \quad [pieces / cm^3] \qquad (3)$$

Since the visual brightness of meteors is a function of meteoroid velocity, the value of d_0 is different for different meteor streams. The function of d_0 to velocity (V) ratio is obtained using the ratio between the visual magnitude of the meteor and the meteoroid velocity [4.2].

This ratio is:

$$lg(d_o) = -0.16 + 0.0025 \cdot V - 0.000125 \cdot V^2 \qquad (4)$$

Substituting the obtained ratio (2) - (4) into the formula (1) we get:

$$\Phi = 0.877 \cdot 10^{14} \cdot r^{-3.6} \cdot 10^{(0.007 \cdot V - 0.00035 \cdot V^2)} \cdot (H.R.) \qquad (5)$$

The total amount of objects which can be registrated during time interval Δt equals $\Phi \cdot \Delta t$. Accounting the fact that objects can pass through different sides of the Earth (therefore relative to the observer), and estimating the efficiency of observing with the radar facilities by the value of coefficient k (k is a fraction of objects which can be in the visual range) we obtain:

$$\nu = k \cdot \Phi \cdot \Delta t \qquad (6)$$

To registrated at least one object during the experiment it is necessary that $\nu > 1$. Since the parameters, determining F, are different for different meteoroid streams, let us consider meteoroid streams which are permanently observed all year round.

Let us consider the condition of visibility of the meteoroid streams during the second part of the 1994 and the first part of 1995. The duration of possible observation of the meteoroid streams is various, so we have assume 7 days as the limiting duration for a single meteoroid observation campaign. We assume the appearance of one at least object during this time.

Besides, as the expected star magnitude is rather low, the observations are impossible during moonlight nights. Taking into the consideration the maximum duration of the observational campaign, radiant co-ordinates and the Moon phases, we calculated the $(H.R.) \cdot \Delta t$ values for the meteoroid streams, which can be observed in the second part of 1994 and the first part of 1995. The value of $(H.R.) \cdot \Delta t$ is the expected amount of objects during the observation time in the observation campaign. Let us denote it below as h (Fig. 4.2).

Table 4.1.

Name	Date of maximum	$(H.R.)\cdot\Delta t$
δ-Aqrds	July, 29	105
Perds	August, 12	1320
Gemds	December, 12	2100
Qdrntds	January, 3	700
η-Aqrds	May, 5	18

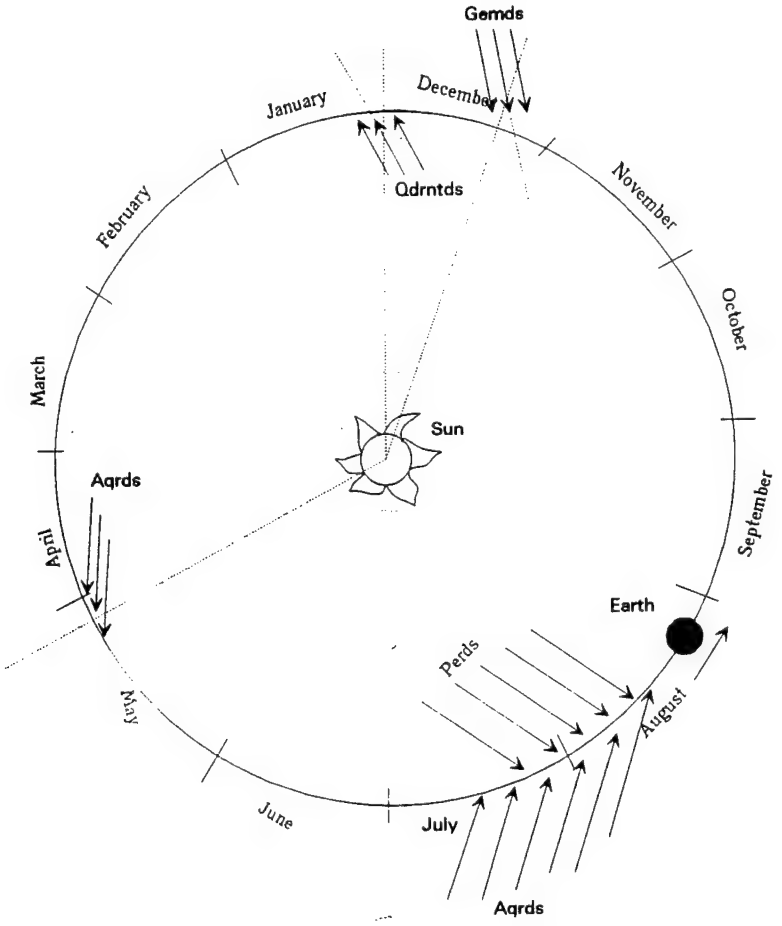

Fig. 4.2. Directions of particle trajectories and periods of some meteor streams relative to the Earth

Let us consider the conditions of the object observations using optical and radar facilities. The suggested experiment consists of the object detecting at the ultimate possible distance of object's approaching to the Earth by the optical facility in order to let the radar facility track it during the passing on the beam of the Earth.

For the optical observations, we assume the object's albedo equal the Moon albedo. Accounting formula (2), the visual star magnitude (m) on the distance R (the optical detecting range) is connected with the sighting distance of passing through the beam of the Earth by:

$$m = 33.0 - 10.0 \cdot \lg(r) + 5.0 \cdot \lg(R) \qquad (7)$$

From formulae (2), (5) - (7) we obtain the estimations for the main parameters of the meteoroid stream for our experiment. Omitting the intermediate formulas, we obtain:

- the sighting distance of the pass on the beam of the Earth:

$$r < 5542 \cdot (h / v)^{1/3.6} \cdot 10^{(0.007 \cdot V - 0.00035 \cdot V^2)/3.6} \quad [km] \qquad (8)$$

- the diameter of the observed object:

$$d < 19.2 \cdot (h / v)^{1/1.8} \cdot 10^{(0.007 \cdot V - 0.00035 \cdot V^2)/1.8} \quad [cm] \qquad (9)$$

- the optical detecting range:

$$R < 7.71 \cdot 10^{0.2 \cdot m} \cdot (h / v)^{1/1.8} \cdot 10^{(0.007 \cdot V - 0.00035 \cdot V^2)/1.8} \quad [km] \qquad (10)$$

- time interval between the moment of detecting and the moment of pass on the beam:

$$t = R/V \ [s] \qquad (11)$$

- the angular radius of the zone of optical search for objects:

$$\varphi = 57.3 \cdot (r / R) \quad [deg] \qquad (12)$$

- the duration of the survey of the zone for object optical search:

$$T = 15 \cdot \varphi^2 \quad [s] \qquad (13)$$

The field of view of the telescope is 1° and the duration of single position observation is 15 sec.

Table 4.2 shows the calculated parameters of the meteor streams when the limiting brightness of optical facility is 16th magnitude.

Table 4.2.

Stream	h	V	r	d	R	t	φ	T
Gemds	2100	35	41250	1060	676700	19340	3.5	183
Perds	1320	61	23300	340	215500	3530	6.2	575
Qdrntds	700	40	28600	510	325000	8120	5.0	381
δ-Aqrds	105	42	16400	170	107800	2570	8.7	1143
η-Aqrds	18	66	6270	25	15850	240	22.7	-

From Table 4.2 it is obvious that only three first streams satisfy the experiment, because for others the duration of search is compatible with the time of approaching.

Positioned optical observations are used to determine the orbit of the approaching object. In order to obtain the orbit elements, at least three observations of object are required. A large number of position observations can be used to improve the accuracy of the orbit determination and, therefore of the co-ordinates. In that case the orbit is calculated using three normal places. The accuracy of these places is higher than the accuracy of the single observation (for a value of a square root of the number of observations used to calculate the normal place). Considering the geometry of the approaching we obtain the connection between the error values for the position optical observations and the errors of co-ordinates δr and $\delta\Theta$. Choosing the co-ordinate system so that the object is moving in general along the Z axis in the XZ plain we obtain that $\delta\Theta = \delta r / r$. Since the motion is executed within specified plain, the angular co-ordinate analogous with the azimuth has a zero value. Let us denote the co-ordinate analogous with the declination by φ.

Let us denote the indexes 0,1,2,3,4,5 to the following time intervals (Fig. 4.3):

t_0 - the moment of the detecting of the object by the optical facility;

t_1 - the first normal point of the position observation;

t_2 - the second normal point of the position observation;

t_3 - the third normal point of the position observation;

t_4 - the moment of the end of optical position observation;

t_5 - the moment of the passing on the beam of the Earth.

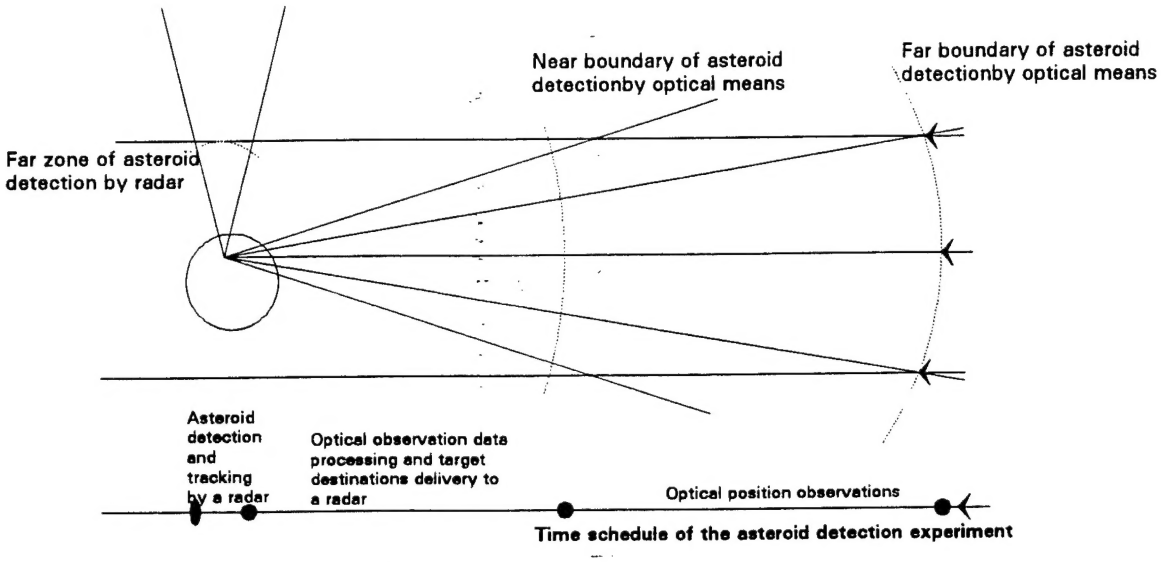

Fig. 4.3. Time and space schedule of asteroid detection experiment.

For the accuracy estimation let us consider that $\Delta t = t_3 - t_2 = t_2 - t_1$, and $t_1 - t_0 > 0.5 \cdot \Delta t$, $t_4 - t_3 > 0.5 \cdot \Delta t$, therefore $t_4 - t_o > 3 \cdot \Delta t$. As $t_5 - t_0 = \Delta t$ (the time interval between the moment of revelation of the object and its passing on the beam of the Earth) and the value of $t_5 - t_4$ is determined by the conditions of the constraint between the optical and radar facilities, and should be rather high, allowing the variable $\mu < 1$, we obtain:

$$\Delta t = (\mu / 3) \cdot t \qquad (14)$$

The value of μ is a fraction of the approaching time used for the co-ordinate measurement by the optical facility.

Taking into account the estimations and the conditions of approaching (choosing the co-ordinate axis) listed above, we obtained the ratio between the errors $\delta\varphi$, $\delta z / r$ and $\delta r / r$, including that $\delta z / r = 1 / 57.3$ and $\delta r / r = 100 / r$. By manipulations on this ratio we get:

$$\delta\varphi = /2 \cdot \mu / 9 \cdot (1 - \mu / 2)/^3 \cdot (r / R) \cdot /(r / R) \cdot (\delta z / r) + (1 + \mu / 2) \cdot (\delta r / r)/ \qquad (15)$$

The calculations for the selected meteor streams shows that if we assume the value of $\mu = 1/2$, the required accuracy of the object co-ordinate determination by the optical facility is 14 arcsec for Gemds, 43 arcsec for Perds and 28 arcsec for Qdrntds. The real position observations using electro-optical facilities have much more accuracy.

Assuming the real accuracy of co-ordinate determination by optical facilities of 3" (single measurement) and 1" (normal point), we get the estimation of μ for the selected meteor streams. This estimation is calculated from formula (15).

Table 4.3 shows: values of μ for the specified accuracy, time intervals necessary to perform the optical position observations $(\mu \cdot t)$, and time intervals remain for the calculations as well as for the co-ordination and communication between the optical and radar observation facilities (τ).

Table 4.3.

Stream	Accuracy $\delta\varphi$	μ	$\mu \cdot t$	τ
Gemds	3"	0.20	3867	15286
	1"	0.09	1740	17413
Perds	3"	0.08	283	2676
	1"	0.03	106	2853
Qdrntds	3"	0.12	975	6767
	1"	0.045	366	7376

In Table 4.3 time is in seconds, μ - is dimensions.

So to Conduct this experiment in the end of 1994 and in the early 1995 tow meteor streams are suitable (their observation periods are: 12th of December for Gemds and 3th of January for Qdrntds).

In 1998 - 2000 the next recycling of the Leonds meteor stream to the Earth is expected (maximum at 16th of November), so this of experiment can supply us with additional information about the population of the objects in the Solar system which are hazardous for the civilisation if they impact the Earth.

1. Detection and Spectrometry of Faint Light /by John Meaburn// D. Reidel Pab.Co., 1976.

2. Astronomical observations - an optical perspective. / by Gordon Walker// Cambrige Univ.Press, 1987.

Conclusion

1. Employment of existing high-potential ground-based radar's, not included into the space surveillance system, enables us to obtain data on small-size (less than 10 cm in diameter) fraction of space debris - and available information on it is quite limited now.

2. Significant input to acquisition of data on the level of pollution of the near-Earth space in medium altitude orbits (5,000 - 25,000 km) can be provided by basic observations done with optical sensors equipped with a complete set of light analysers, which will support both positioned measurements and all kinds of non-co-ordinate measurements.

3. Detection of asteroids with the size of $\approx$ 10 m and more in principle is possible not only by optical sensors, but by existing radar's as well (in case respective target designation inputs are provided). To conduct an integrated experiment with employment of both optical and radar assets it is most suitable to observe in the near future two meteor streams: the Jemenides - on December 12, 1994 and the Quadratides - on Januari 3, 1995.